2014

Overtone Spectroscopy of Hydrogen in MOF-5

Jocienne N. Nelson
Oberlin College

OBERLIN COLLEGE

Overtone Spectroscopy of Hydrogen in MOF-5

by

Jocienne N. Nelson

in the

Physics and Astronomy Department

May 2014

Acknowledgements

First and foremost I would like to thank my adviser Professor Stephen FitzGerald for his advice and support, for always making time to answer my questions and for showing me how fascinating, frustrating and rewarding experimental physics can be. I am grateful for the opportunity to pursue this work which has been a significant and enjoyable part of my time at Oberlin.

I thank my labmates past and present: Jenny Schloss, Chris Pierce, Sujoy Bhattacharyya, Benjamin Lemberger, Noah Jones, Elizabeth Gilmour, Clay Hudgens and Cooper McDonald for interesting and helpful conversations and fun times in lab.

Many thanks to Professor Jesse Rowsell for synthesizing our MOFs and for his helpful conversations and insights into the structure and behavior of these materials.

I thank Professor Jason Stalnaker for his advice and for teaching me much of the physics I know now.

I thank Ben for being a great friend and for wonderful conversations about physics and life. I thank my fellow physics students including but not limited to Kathryn Hasz, Zachary Mark, Chetan Poudel, David Morris, Elizabeth Garbee, Kara Kundert, Mattie DeDoes, Dagmawi Gebreselasse, Michael Rowan, and Greg Stevens for their friendship and company which made even all night problem sets not only bearable but great fun.

I would like to thank Donald Nelson for invaluable help proof reading.

I thank my family without whose support none of this would be possible.

Contents

List of Figures

List of Tables

Glossary

Absorption - Interaction of light with matter in which energy is taken up. In this thesis absorption refers to an infrared light source causing a change in the energy levels of the hydrogen molecule or the MOF material.

Adsorption - surface van der Waals or dipole dipole interactions between molecular hydrogen and the materials which trap it.

cm^{-1} - Wavenumbers defined as inverse wavelength in spectroscopic applications $1/\lambda$. Wavenumbers are used as a unit of energy in this thesis using the relationship E = hc/λ. Wavenumbers can be converted into temperature (in Kelvin) using the relationship E = k_BT where k_B is Boltzmann's constant 1 cm^{-1} = 1.439 K.

Energy Units - Other units of energy useful in this thesis are meV and kJ/mol which are commonly used to describe the binding energy of a hydrogen molecule to a MOF material. Using similar conversions through energy 1 meV = 11.604 K and 1 kJ/mol = 120.3 K.

Hydrogen - In this thesis hydrogen is used to refer to all isotopologues in general. H_2, HD and D_2 is used to refer to each isotopologue specifically. An isotope is an atom that differs in the neutron number while having the same proton number, i.e. H and D are isotopes. An isotopologue is a molecule that differs only in its isotope content.

MOF - Metal-Organic Framework, a nanoporous crystalline material, made up of metal atoms connected by aromatic linkers.

S peaks - Peaks in intensity associated with rotational transitions where the rotational quantum number increases by two, $\Delta J = +2$, in addition to a vibrational transition.

Q peaks - Peaks in intensity associated with vibrational transitions where only the ν quantum number changes and Δ J = 0.

Executive Summary

Metal-organic frameworks or MOFs are adsorbent nanoporous materials made out of metal atoms and organic linker molecules. They are highly tailorable molecular structures which accommodate a large amount of modification. They are promising for applications such as gas storage and gas separation. Global climate change is a pressing issue that requires clean energy technologies to power processes like transportation. The burning of fossil fuels in cars contributes to the increasing amounts of greenhouse gases in the atmosphere. Alternative methods of storing and transferring energy, like hydrogen, are needed. However the problem of storing such gases is unsolved since high pressure gas tanks are both heavy and dangerous and thus not a feasible option. One possible solution is to use adsorbent materials which hydrogen will 'stick' to in order to achieve dense storage without high pressures. Metal-Organic Frameworks or MOFs are one such class of materials. Since no ideal MOF material for storage exists so it is necessary to study the gas-MOF interactions to better understand them and learn enough to build a practical structure.

Metal-organic frameworks have also been shown to be more immediately useful for gas separation applications. In his thesis Chris Pierce [1] studied the possibilities for hydrogen isotope separation in the material known as MOF-74 via gas adsorption measurements. This study confirmed that MOF-74 is promising for isolating deuterium, a rare and useful isotope of hydrogen, used in scientific, medical and nuclear applications [2]. Recently others have experimentally confirmed this possibility [3]. To extend this work we have developed methods to study the dynamics of all trapped isotopes. In this thesis we study the prototypical material called MOF-5. We use infrared spectroscopy to study the frequencies of light absorbed by trapped hydrogen molecules. MOF-5 is one of the most studied and best understood of the metal-organic frameworks. Thus it is an ideal system in which to test our technique of overtone spectroscopy. Molecules, like musical instruments have higher harmonics or overtones one of which occurs at twice the fundamental frequency or an octave above the original note. The overtones are usually much weaker than the fundamental frequencies. However in our MOF-5 system they are stronger than predicted by theory developed for gas phase hydrogen, indicating a significant change in the molecule from gaseous form. The overtone spectrum stands out clearly and provides a new tool to study the trapped molecules' behavior. It greatly aids our study of hydrogen isotopes which without overtone spectroscopy is prohibitively challenging. This will add to the understanding of metal-organic frameworks and aid in the quest to develop new materials for isotope separation, hydrogen storage and other applications.

Chapter 1

Introduction

1.1 Motivation

Global climate change is a pressing worldwide problem which most scientists agree is caused primarily by human activities These include the burning of fossil fuels for processes such as transportation [4]. It is an important scientific challenge to devise new ways of powering transportation that do not add to the amount of greenhouse gases in the atmosphere. Molecular hydrogen offers much promise in the practical transportation of energy. It could allow energy from renewable sources like wind to be used in cars and other applications. It acts as an ideal energy carrier in a closed cycle with no polluting by-products. Water is separated into H_2 and O_2 by hydrolysis. The H_2 is then stored in some material for use in a fuel cell which produces energy through oxidation and only releases water vapor. One kg of H_2 can release more energy than 7 kg of coal or 3 kg of gasoline [5]. However as H_2 is a gas at room temperature it has a huge volume and requires a condensed storage form. High pressure storage is dangerous and heavy; liquid storage requires cooling to extremely low temperatures, below 20 K [6]. Thus much research is devoted to fabricating new materials to trap hydrogen directly from gas form. The Department of Energy has stated targets for the capacities for H_2 storage materials: of 7.5 % wt for gravimetric density, and 70 g/L for volumetric density [7].

Possible materials which have been proposed to solve this problem include solid-state materials such as metal hydrides, metal-organic frameworks (MOFs) and zeolites [5]. In these materials the hydrogen is either disassociated and stored in atomic form, where it is bonded to the material, or stored through physisorption where the hydrogen retains its molecular form. Much work has gone into exploring the possibilities for solid-state storage [5, 8, 9]. The disadvantage of atomic hydrogen storage used in materials such as metal hydrides is that the material must be heated to hundreds of °C before hydrogen is

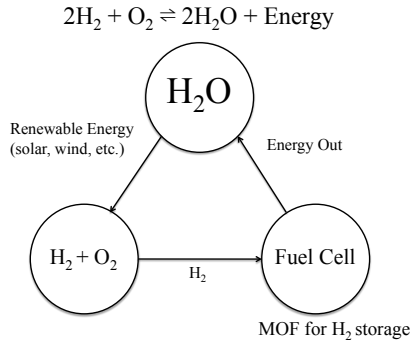

FIGURE 1.1: The closed cycle reaction involved in using H_2 as an energy carrier.

released. This makes it impractical especially for mobile applications [8]. Metal-organic frameworks use the second mechanism of molecular storage. While they cannot store hydrogen at room temperature and require cryogenic cooling for storage, they are as a consequence able to desorb hydrogen without heating. MOFs in general are an exciting avenue of investigation because of their potential to be tuned for specific applications which go beyond storage to include gas separation and catalyzation.

Another application for MOFs which is of much theoretical and practical interest is isotopologue separation. In his thesis Chris Pierce [1] explored the possibility of H_2, D_2 separation using the isostructural series of materials M-MOF-74 (M = Mg, Mn, Fe, Co, Ni, Zn). Isotopologue separation is extremely challenging since it cannot rely on size differences, or charge differences. In hydrogen the only significant difference between isotopologues for the purpose of separation is the mass. Deuterium is desirable to isolate as it is extremely useful for both scientific and medical applications and is used in nuclear reactors. The current method of separation is electrolysis of D_2O or heavy water produced using the Girdler Sulfide process with a selectivity of 1.6 [2]. FitzGerald et. al. predicted a selectivity of 5 at 77 K using the preferential absorbance of D_2 in the material known as Ni-MOF-74 due to its lower zero point energy . More recently Oh et. al. [3] have demonstrated an enrichment of D_2 from 5% to 95% over a three cycle process using the material Co-MOF-74. These results are promising and, as the authors of ref [3] comment, will hopefully lead to the development of nanoporous materials with higher selectivities in order to achieve separation at higher temperatures. However in order to build such materials the isotopologue effect must be understood in more detail. While infrared spectroscopy is an excellent way of probing the quantum mechanical behavior of hydrogen in MOFs it is complicated by the fact that many of the transitions coincide with IR peaks from the MOFs themselves particularly for the isotopologue D_2 (Fig. 1.2). In this thesis I present overtone spectroscopy using diffuse reflectance infrared Fourier transform spectroscopy (DRIFTS) as a method for avoiding this coincidence

and for studying all isotopologues of hydrogen. Fortuitously the overtone technique is most sensitive to hydrogen bound at the primary or metal site which is the structural feature responsible for selectivity.

1.1.1 Metal-Organic Frameworks

Metal-Organic Frameworks are an exciting new class of materials that have the potential to solve these challenging problems in gas storage and contribute to available technology for gas separation and catalysis. They are made out of metal complexes linked by organic chains to form highly complex crystalline structures with many pores available for gas sequestration and adsorption. Their multiple adsorption sites and large internal surface areas allow them to densely store gases without dangerously high pressures that occur in gas tanks. In principle it is possible to choose the metal and linker to make the ideal MOF structure for a specific application [10]. Much work has been done on evaluating MOFs for their practical possibility for hydrogen storage [10–12]. However many requirements are unsatisfied for a practical storage material, perhaps most importantly creating a material with a large enough binding energy for hydrogen so that it can store gas at room temperatures and comply with the Department of Energy targets [7]. Presently no existing material is adequate, so new materials must be discovered and synthesized. Since there are so many possible MOF structures it is impractical to build all of them. Theoretical work is being done to attempt to understand the gas MOF interactions [13]. Infrared measurements of the spectrum of adsorbed molecules have the possibility to be important input for computational models and have already been used to motivate theory [14].

1.1.2 Overtone

The fundamental spectrum of adsorbed hydrogen consisting of peaks due to transitions from the vibrational ground to first excited state in various metal-organic frameworks has been extensively studied [15–20]. The overtone spectrum, or vibrational ground to second excited state transition, has been less studied. The adsorbed hydrogen signal is small even in the fundamental region. Since the overtone transitions only arise from small deviations of the hydrogen molecule from simple harmonic behavior either in the internuclear potential or the wavefunction (section 3.2.1.3) they are expected to be much weaker. Thus many techniques cannot detect it in the overtone. This is due to the large reduction of the intensity of overtone peaks relative to the fundamental. The intensity of the overtones is predicted to be about 2-5% of the intensity of the fundamental for

gas phase H_2 (Ch. 6). Experimental study of the overtone in gas phase hydrogen [21–23] and on hydrogen trapped in zeolites [24–26] has been done but suffers from weak intensity in the gas phase and inability to resolve peaks in zeolites. However the overtone is worth the effort of detection as we show in this thesis because it adds information to the picture of hydrogen dynamics. The great advantage the overtone is that it is unlikely to overlap with any peaks due to the MOF material (Fig. 1.2). As a consequence it has the potential to resolve ambiguities in peak assignment which exist in the fundamental spectrum. Furthermore the overtone can reveal information about hydrogen molecule itself due to the discrepancies between standard theory for free hydrogen and observed hydrogen behavior in the MOF.

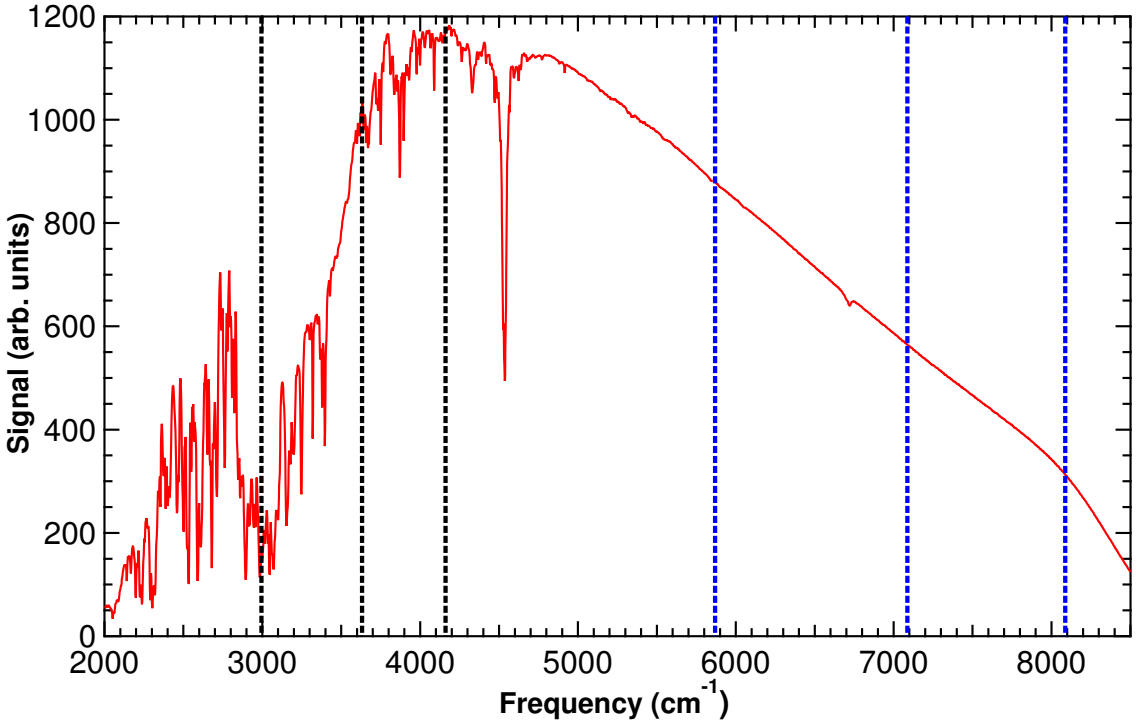

FIGURE 1.2: A raw spectrum of MOF-5 taken using the MCT detector. The fundamental gas phase frequencies for H_2, HD and D_2 are shown as black dotted lines while the overtone gas phase frequencies are shown in blue. This spectrum demonstrates the advantage of studying the overtone region where there are no MOF-5 peaks.

1.2 Outline

In chapter 2 we introduce the material used in this study, MOF-5, and explain why it was chosen. In chapter 3 we present the necessary background theory for this work. In chapter 4 we describe our experimental setup, procedure, and the modifications from previous experiments necessary for overtone spectroscopy. In chapter 5 we present the

bulk of our results which demonstrate the promise of overtone spectroscopy. In chapter 6 we explore the change in the nature of the hydrogen spectrum in the overtone which informs us about the binding of the hydrogen to the metal site. In chapter 7 we describe future work. Finally we conclude this thesis in chapter 8.

Chapter 2

MOF-5

2.1 Introduction to MOF-5

The nanoporous crystalline structure known as MOF-5 or isoreticular metal organic framework 1 (IR-MOF-1) is a prototypical example of a metal organic framework. It has been extensively studied and is a good candidate for industrial applications. The location of gas molecules loaded in MOF-5 has been probed through both neutron diffraction [27, 28] and x-ray diffraction [29]. Adsorption isotherms have been used to study gas uptake [30]. MOF-5 has aroused interest for its high capacity for hydrogen storage, by weight up to 11 % measured at 3.5 K [28]. This is the highest to date of any MOF. It has a cubic structure shown in Fig. 2.1 with the formula unit $Zn_4O(BDC)_3$. The framework is made of Zn_4O clusters at the vertices of the cube, connected by 1, 4-benzenedicarboxylate (BDC) linkers. It is synthesized using wet chemistry techniques first described by Li et. al. [31]. Due to the geometry of the metal clusters MOF-5 has alternating pore sizes (Fig. 2.2). The location of adsorbed hydrogen in this structure has been probed using neutron diffraction of deuterium loaded in MOF-5 [28]. In neutron diffraction D_2 is used rather than H_2 due to the large incoherent scattering cross section of H_2. Multiple binding sites for hydrogen have been identified in the structure. This includes the primary metal site (also known as the α site or cup site) which is positioned at the corners of the large pores. The Zn_4O clusters form tetrahedrons at the corners of the cube. Each face of a tetrahedra makes up a primary site which is associated with three equidistant Zn atoms and thus has three-fold symmetry (Fig. 2.3). The metal has the largest binding energy of all hydrogen sites and thus is likely to be occupied first. In principal at low enough temperatures the metal site would be totally occupied before any other sites. Our previous infrared study of hydrogen in MOF-5, summarized in FitzGerald et. al. [15] and in Hopkins' thesis [32], estimated a binding energy of 4

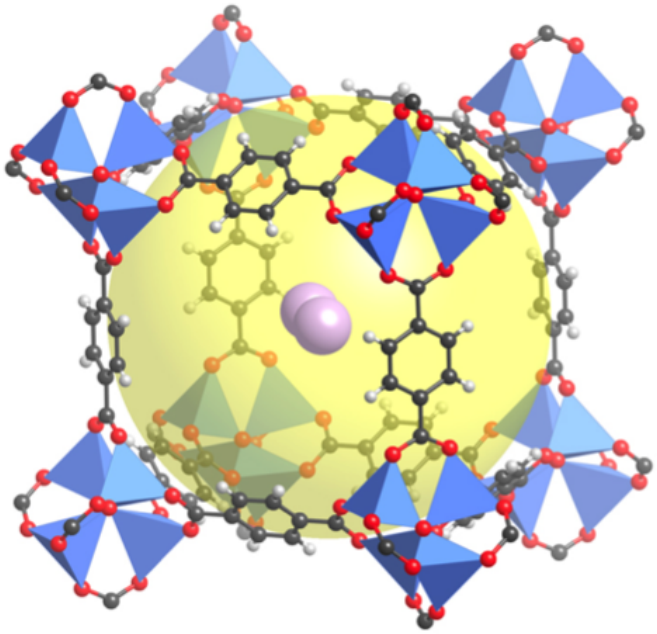

FIGURE 2.1: A partial MOF-5 unit cell. The boundaries of the unit cell bisect the linking molecules which form the sides of the cube. The oxygen atoms (red) at the centers of metal clusters which make up the vertices of the pore. The base oxygens are positioned at (1/4, 1/4), (1/4, 3/4), (3/4, 1/4) and (3/4, 3/4). Thus the side length of the cubic pore is half the length of a unit cell. The Zn_4O tetrahedra at the vertices of the cube and hold the primary sites for gas adsorption. The blue tetrahedrons represent Zn, oxygen is shown in red, carbon is black, and the hydrogen atoms that are part of the structure are gray. The yellow sphere indicates the open space for adsorbed molecules. Image courtesy of Jesse Rowsell.

kJ/mol for the primary site and 3 and 2.5 kJ/mol for two of the other observed sites or secondary sites. The secondary sites are associated with other parts of the structure including a ZnO_3, ZnO_2, and the Benzene ring on the aromatic linker [28]. This energy difference corresponds to an equivalent temperature, k_BT, on the order of 100 K , where k_B is Boltzmann's constant. Density functional theory calculations based on neutron diffraction predict a larger binding energy for all sites than what we observe using infrared spectroscopy but agree with infrared measurements that the relative binding energies of the secondary sites being 65-70% of the binding energy of the primary site[28].

MOF-5 is the obvious candidate to test an overtone spectroscopy approach to analyzing hydrogen dynamics. In addition to being of practical importance and so well characterized it also has some of the sharpest and most well defined transition peaks both in infrared spectroscopy and inelastic neutron scattering [33] which similarly to infrared can probe the dynamics of trapped hydrogen. Additionally the fundamental spectrum of hydrogen in MOF-5 has been analyzed theoretically [14]. Since the fundamental spectrum of MOF-5 is well known it is an ideal starting point for studying the overtone spectrum.

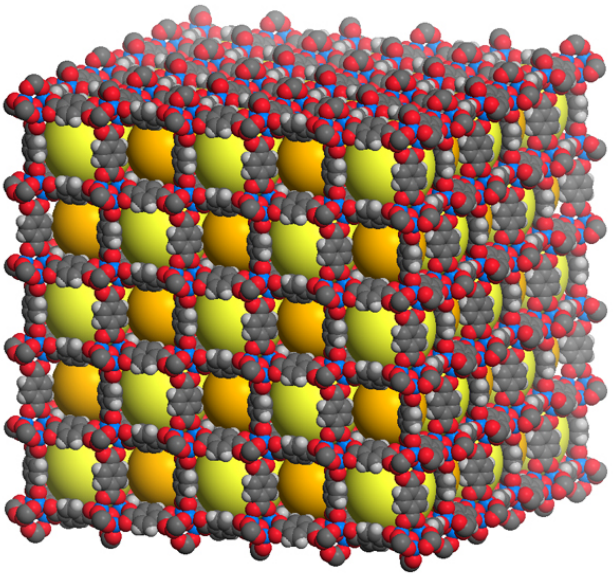

FIGURE 2.2: Space filling representation of MOF-5 structure. Large pores are represented as yellow spheres and smaller pores represented as orange. MOF-5 has a face-centered cubic structure. While the vertices of the unit cell do not correspond to any atom position, the pores can be thought of as making up the structure either as a face-centered cubic with large pores in the middle and midpoints of sides and small pores on the vertices and faces or as an intersecting simple cubic lattice made up of the two types of pores, similar to NaCl structure. Image Courtesy of Jesse Rowsell.

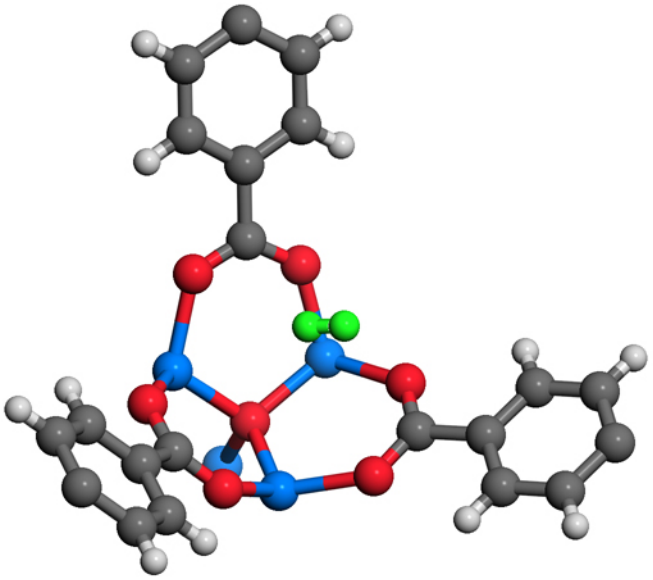

FIGURE 2.3: MOF-5 primary metal site. The metal site is at the corner of large pores. Here hydrogen is equidistant from three Zn atoms and experiences a potential surface with three-fold symmetry. Image Courtesy of Jesse Rowsell.

Chapter 3

Theory

3.1 Infrared Transitions

Infrared spectroscopy uses infrared light to study a molecule or material. To first approximation this is the interaction of light with the electric dipole moment, or separation of charge, of a molecule. It is possible to study interactions with the magnetic dipole moment and the quadrupole moment but the probability of transitions due to these effects are 10^{-5} and 10^{-8} relative to transitions due to the electric dipole moment [34] thus negligible.

3.1.1 Transition Probability

The wavelength of infrared light is approximately 7000 - 10,000 Å while the size of a molecule like hydrogen is only a few Å. Thus the photon can be viewed as a spatially homogeneous oscillating electric field over the length scale of the molecule:

$$E = E_0 cos(\omega t)\hat{k}. \tag{3.1}$$

For simplicity let the photon be polarized along the z direction. The effect of the light is treated as a perturbation to the Hamiltonian of the hydrogen molecule - which is either free or in some material potential (following Griffiths ch. 9.1 - 9.2 [35]). Since the potential energy of a charged particle in an electric field is $U = -\int F \cdot dr = -\int qE_0 cos(\omega t)dz$, the perturbation is:

$$H' = -qE_0 z cos(\omega t). \tag{3.2}$$

From Griffiths the transition probability from one state to another where the states are orthonormal ($\langle\psi_i|\psi_f\rangle = \delta_{if}$) for a perturbation with sinusoidal time dependence is:

$$P_{i\to f}(t) = \frac{|V_{if}|^2}{\hbar^2}\frac{sin^2[(\omega_0-\omega)t/2]}{(\omega_0-\omega)^2}. \tag{3.3}$$

The sinusoidal term indicates that there is time dependence and that transitions caused by photons with frequency ω far from the transition frequency ω_0 are unlikely. The constant V_{if} is defined as:

$$V_{if}cos(\omega t) = \langle\psi_i|H'|\psi_f\rangle = -E_0cos(\omega t)\,\langle\psi_i|qz|\psi_f\rangle\,, \tag{3.4}$$

where qz is the dipole moment. For molecules it is necessary to sum over all charges of the molecule. Thus it is apparent that the transition probability is proportional to:

$$P_{i\to f} \propto \left|\langle\psi_i|qz|\psi_f\rangle\right|^2. \tag{3.5}$$

Since it is given that the states are orthonormal and $i \neq f$ only transitions that involve a change in the dipole moment qz are observed since if no change occurs we find that:

$$\langle\psi_i|qz|\psi_f\rangle = 0. \tag{3.6}$$

3.2 Hydrogen Dynamics

Hydrogen is a diatomic molecule that can be thought of as two masses on a spring. The characteristic motions of hydrogen are vibration, rotation and center of mass translation. A full picture of the motion is described by six coordinates. The internuclear separation, ρ, the rotational coordinates θ and ϕ and the center of mass location X, Y and Z. First hydrogen will be treated as a simple harmonic oscillator. Then the rotational dynamics will then be analyzed with the rotating dumbbell model. The anharmonic qualities of hydrogen and the origin of the overtone transitions are then be explored. Then the vibrating rotor model will then be introduced. Finally the translational motions will be described.

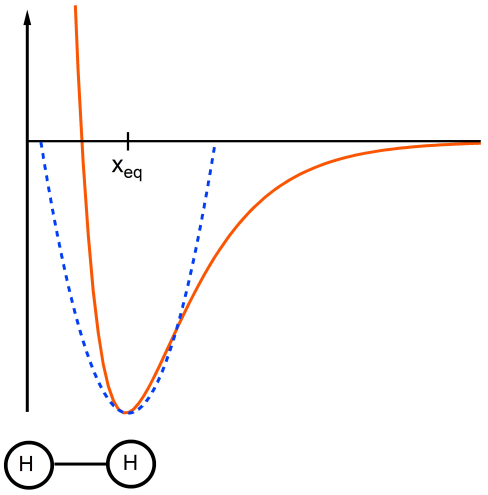

FIGURE 3.1: The potential experienced by one hydrogen atom in the frame of the other. The simple harmonic potential, in blue, is a good approximation at small deviations from equilibrium separation. The Morse potential, in red, describes the anharmonic motions of diatomic molecules.

3.2.1 Vibrations

3.2.1.1 Simple Harmonic Potential

Any potential U(x) can be Taylor expanded about a local minimum which is a stable equilibrium (Fig. 3.1). Since neither the potential of hydrogen in the MOF or in the gas phase is known exactly such approximations are useful. The potential is Taylor expanded:

$$U(x) = U(x_{eq}) + \left.\frac{dU}{dx}\right|_{x_{eq}} (x - x_{eq}) + \frac{1}{2}\left.\frac{d^2U}{dx^2}\right|_{x_{eq}} (x - x_{eq})^2 + ..., \tag{3.7}$$

x is the separation of the atoms and x_{eq} is the equilibrium separation. The first term in the expansion is a constant and can be neglected, the second term is zero since $\frac{dU}{dx}$ is zero at extrema. The third term is the simple harmonic oscillator potential where the effective spring constant is defined as $k = \left.\frac{d^2U}{dx^2}\right|_{x_{eq}}$.

Since the potential is only dependent on the separation of atoms one can freely choose which frame to solve for the equations of motion. For simplicity the center of mass frame is chosen. Thus it is appropriate to introduce the reduce mass:

$$\mu_{H_2} = \frac{m_H m_H}{m_H + m_H} = \frac{m_H}{2}, \tag{3.8}$$

The Lagrangian is:

$$\mathscr{L} = \frac{1}{2}\mu\ddot{x} - \frac{1}{2}k(x - x_{eq}), \tag{3.9}$$

solving the Euler-Lagrange equation obtains the familiar equations of motion for a simple harmonic oscillator:

$$x = Acos(\omega t) + BSin(\omega t), \tag{3.10}$$

where the frequency of oscillation ω is equal to $\sqrt{\frac{k}{\mu}}$.

The frequencies of oscillations for the various isotopologues scale with the reduced mass:

$$\mu_{D_2} = \frac{2m_H 2m_H}{2m_H + 2m_H} = mH = 2\mu_{H_2}, \tag{3.11}$$

$$\mu_{HD} = \frac{2m_H m_H}{2m_H + m_H} = \frac{2m_H}{3} = \frac{4\mu_{H_2}}{3}. \tag{3.12}$$

Since the experimentally observed frequency of hydrogen in the gas phase is about 4161 cm^{-1} [36] the frequency of deuterium should be about 2942 cm^{-1} and the frequency of hydrogen deuteride (HD) about 3604 cm^{-1}. These are slightly different from the actual values of 2994 cm^{-1} and 3632 cm^{-1} [37] but this makes sense given that the simple harmonic potential is only a first order approximation. Griffiths [35] solves for the energy levels of the 1 dimensional simple harmonic oscillator to find:

$$E_n = \left(n + \frac{1}{2}\right)\hbar\omega \tag{3.13}$$

where n is the vibrational quantum number, $\hbar$ is Planck's reduced constant and ω is again the frequency of oscillation.

3.2.1.2 Simple Harmonic Transitions

Infrared spectroscopy is in the correct frequency regime to look at transitions between different vibrational energy levels of the hydrogen molecules. As shown in section 3.1.1 the intensity of a transition is proportional to $\left|\langle\psi_i|\mu|\psi_f\rangle\right|^2$, where ψ_i is the initial state of the hydrogen, ψ_f is the final state and μ is the dipole moment of the system. The dipole moment is written as a separation of charge, i.e. as a charge, q, times a distance x:

$$\mu = qx \tag{3.14}$$

The distance, x, is rewritten using ladder operators (see Griffiths' Quantum Mechanics [35]):

$$x = \sqrt{\frac{\hbar}{2m\omega}}\,(a_+ + a_-)\,. \tag{3.15}$$

$$a_+\psi_n = \sqrt{n+1}\;\psi_{n+1} \tag{3.16}$$

$$a_-\psi_n = \sqrt{n}\;\psi_{n-1} \tag{3.17}$$

Now it is possible to explore what transitions between hydrogen energy levels are expected. The hydrogen molecule is very unlikely to be in an excited state before being perturbed by a photon. According to Maxwell-Boltzmann statistics the probability is:

$$P = e^{-\Delta E/k_B T}, \tag{3.18}$$

where k_B is Boltzmann's constant, T is the temperature and ΔE is the difference in energy between the ground and first vibrational states which is about 4161 cm^{-1} for gas phase hydrogen. Thus the probability of being in the first excited state is $P = e^{-4161\times 1.44/k_B T}$, which is about 4.5×10^{-75} at 35 K, our usual experimental temperature. The factor 1.44 converts from wavenumbers to kelvin. Our experiments occur at low enough temperatures so that it is appropriate to neglect transitions from states other than the vibrational ground state.

Consider a vibrational ground to excited state transition whose intensity depends on:

$$\langle \nu = 0 | qx | \nu = n \rangle \tag{3.19}$$

where we have adopted the notation where $\nu = n$ stands in for ψ_n which is the wavefunction of the simple harmonic oscillator in the nth state. We can now rewrite x using ladder operators:

$$\langle 0 | q \sqrt{\frac{\hbar}{2m\omega}}\,(a_+ + a_-)\,|n\rangle \tag{3.20}$$

$$\langle \nu = 0 | q \sqrt{\frac{\hbar}{2m\omega}} \left(\sqrt{n+1}\;\; \nu = n+1 \;\; + \;\; \sqrt{n}\;\nu = n-1 \right) \rangle\,. \tag{3.21}$$

We can take the constant out in front and thus get:

$$q \sqrt{\frac{\hbar}{2m\omega}} \left(\sqrt{n+1}\;\; \langle \nu = 0 | \nu = n+1 \rangle + \;\sqrt{n}\,\langle \nu = 0 | \nu = n-1 \rangle \right). \tag{3.22}$$

We know from standard orthogonality conditions that:

$$\langle \nu = n | \nu = m \rangle \quad = \delta_{nm} \tag{3.23}$$

thus $\langle \nu = 0 | \nu = n+1 \rangle = 0$ and $\langle \nu = 0 | \nu = n-1 \rangle = 1$ when $n = 1$ so Eq. (3.19) becomes:

$$\langle \nu = 0 | qx | \nu = 1 \rangle = q\sqrt{\frac{\hbar}{2m\omega}} \tag{3.24}$$

and the fundamental is the only visible transition.

Thus the overtone transition $\langle \nu = 0 | qx | \nu = 2 \rangle$ is zero because of orthogonality. However overtones are experimentally observed. They are consequences of the deviation of the hydrogen potential from simple harmonic behavior. This is equivalent to going out to higher terms in the Taylor expansion (Eq. 3.7).

3.2.1.3 Anharmonic Oscillator

The Dunham expansion is used as an example of an anharmonic potential (for more details on this expansion refer to ch. 1 of Townes' Microwave Spectroscopy [38] which this discussion relies on). This expansion is just a modified version of equation 3.7:

$$U(\xi) = a_0(\xi^2 + a_1\xi^3 + a_2\xi^4 + ...). \tag{3.25}$$

The first two terms of the Taylor expansion have been neglected as being a constant and zero. Here ξ is a dimensionless quantity defined as:

$$\xi = \frac{r - r_e}{r_e}, \tag{3.26}$$

where r_e is the equilibrium separation of a diatomic molecule. When we solve the Schrödinger equation for this potential we find that the energy levels are:

$$E(\nu, J) = \omega_e(\nu + \frac{1}{2}) - \omega_e x_e(\nu + \frac{1}{2})^2 + \omega_e y_e(\nu + \frac{1}{2})^3 + ..., \tag{3.27}$$

where ω_e, $\omega_e x_e$,and $\omega_e y_e$ are molecular constants.

The solutions for the vibrational wavefunctions can now be written in terms of the wave functions of the simple harmonic oscillator, following ref [22].

$$\begin{aligned} |\nu = 0\rangle = |n = 0\rangle + A(-3\,|n = 1\rangle - \frac{1}{3}\sqrt{6}\,|n = 3\rangle) \\ + B(-3\sqrt{2}\,|n = 2\rangle - \frac{1}{2}\sqrt{6}\,|n = 4\rangle), \end{aligned} \tag{3.28}$$

$$
\begin{aligned}
|\nu = 1\rangle = |n = 1\rangle & \\
&+ A(3\,|n = 0\rangle - 6\sqrt{2}\,|n = 2\rangle - \frac{2}{3}\sqrt{6}\,|n = 4\rangle) \\
&+ B(-5\sqrt{6}\,|n = 3\rangle - \frac{1}{2}\sqrt{30}\,|n = 5\rangle),
\end{aligned} \tag{3.29}
$$

$$
\begin{aligned}
|\nu = 2\rangle = |n = 2\rangle & \\
&+ A(6\sqrt{2}\,|n = 1\rangle - 9\sqrt{3}\,|n = 3\rangle - \frac{2}{3}\sqrt{15}\,|n = 5\rangle) \\
&+ B(3\sqrt{2}\,|n = 0\rangle - 14\sqrt{3}\,|n = 4\rangle - \frac{3}{2}\sqrt{10}\,|n = 6\rangle).
\end{aligned} \tag{3.30}
$$

Here $|\nu\rangle$ refers to the vibrational eigenstate of the hydrogen molecule and $|n\rangle$ refers to the wavefunction ψ_n of the simple harmonic oscillator. The constants A and B are defined as:

$$A = \frac{1}{4}a_1\left(B_e/\omega_e\right)^{1/2} \tag{3.31}$$

$$B = \frac{1}{4}a_2\left(B_e/\omega_e\right) \tag{3.32}$$

Now the existence of overtones can be addressed. The expansion in terms of simple harmonic oscillator wavefunctions allows the convenient method of ladder operators to be used. The probability of observing an overtone transition is proportional to $\left|\langle\nu = 0|qx|\nu = 2\rangle\right|^2$. It is obvious that there are terms of the nature: $\langle\nu|qx|\nu \pm 1\rangle$ which are nonzero. Now that the wavefunctions are no longer simple harmonic solutions and instead a mixture of simple harmonic eigenstates there is also a nonzero predicted intensity for the overtone in anharmonic potentials.

3.2.2 Rotations

3.2.2.1 Rigid Rotor

The rotations of the hydrogen molecule are now considered. As a first approximation the hydrogen molecule is a rotating dumbbell with no vibrational motion and classical energy:

$$E_{rot} = \frac{L^2}{2I}, \tag{3.33}$$

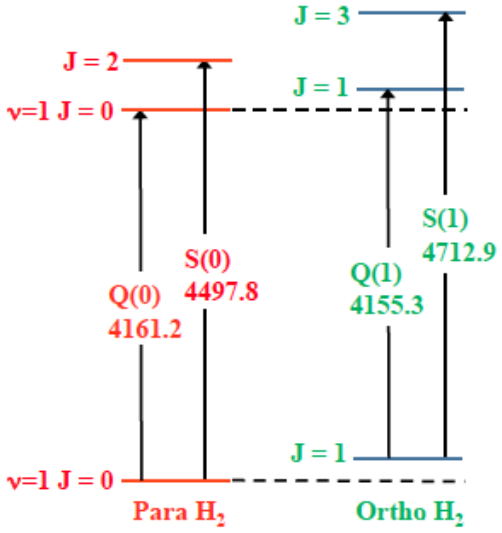

FIGURE 3.2: Schematic of vibrational and rotational transitions: Q refers to vibrational transitions associated with changes in the quantum number ν, S refers to rotational transitions associate with changes in the quantum number J. All numbers refer to observed frequencies of transition in gas phase hydrogen [15]. Para hydrogen is H_2 with total spin 0 and ortho is H_2 with total spin 1. In accordance with infrared selection rules of molecules in electric fields only transitions where $\Delta J = 0$ or $\Delta J = 2$ are allowed.

where L is the angular momentum of the dumbbell and I is the moment of inertia. Knowing from quantum mechanics that:

$$L^2 f_J^m = \hbar^2 J(J+1) f_J^m, \tag{3.34}$$

where J is the rotational quantum number and f_J^m is the angular part of the wavefunction described by a linear combination of spherical harmonics, it is possible to find the energy levels of the rigid rotor:

$$E_J = BJ(J+1). \tag{3.35}$$

Here B is the rotational constant and is defined in the spectroscopic unit of wavenumbers cm^{-1} as:

$$B = \frac{h}{8\pi^2 Ic}, \tag{3.36}$$

where h is Planck's constant, I is the moment of inertia and c is the speed of light. The constant B_{H_2} is approximately 60 cm^{-1} for hydrogen and since the moment of inertia for diatomic molecules scales as the reduced mass and the separation of the nuclei are approximately the same for all isotopologues, it is immediately apparent that $B_{D_2} \approx 30$ cm^{-1} and $B_{HD} \approx 45$ cm^{-1}. This predicts that pure rotational transitions for H_2 are about 360 cm^{-1} for J $_{0\to2}$, 600 cm^{-1} for J $_{1\to3}$, thus far out of our range of sensitivity.

Transitions from excited states, other than J=1 (as described in section 3.4), are again unlikely to be seen. Boltzmann statistics predicts a probability of being in the J=2 excited level rather than the J=0 level of 6.1×10^{-4} for D_2, 1.5×10^{-5} for HD, and 2.7×10^{-7} for H_2.

3.2.2.2 Vibrating Rotor

Experimentally we observe rotational transitions combined with vibrational transitions. Thus it is now appropriate to consider the effects of a vibrating and rotating molecule using a modified version of the Dunham expansion from section 3.2.1.3:

$$U(\xi) = a_0(\xi^2 + a_1\xi^3 + a_2\xi^4 + ...), + U_{cd}(\xi) \tag{3.37}$$

where $U_{cd}(\xi)$ is a correction due to the rotations:

$$U_{cd}(\xi) = a_0 4J(J+1)\left(\frac{B}{\omega_e}\right)^2(1 - 2\xi + 3\xi^2 - 4\xi^3 + ...). \tag{3.38}$$

It accounts for the modification of the potential the hydrogen experiences based on what rotational state the molecule is in. The energy levels are also modified to account for rotational excited states:

$$E(\nu, J) = \omega_e(\nu+\frac{1}{2}) - \omega_e x_e(\nu+\frac{1}{2})^2 + \omega_e y_e(\nu+\frac{1}{2})^3 + ... + B_e J(J+1) - \alpha_e(\nu+\frac{1}{2})J(J+1) + ..., \tag{3.39}$$

where α_e is another molecular constant.

3.2.3 Translational Motion

The one motion we have left to address is the hydrogen translational or center of mass motion. This is the motion of the whole molecule in three dimensional space described by the coordinates X, Y, Z. The translational peaks are not a dominating feature in the MOF-5 spectrum and are weaker in intensity than the vibrational-rotational peaks, but we include them here for completeness. At each binding site the hydrogen experiences both an attractive van der Waals term due to dipole-dipole interactions and a repulsive term that prevents electronic overlap. This term depends on a sum over the whole MOF structure and thus is complicated and not known well. The combination of the two terms is commonly approximated using the simple Lennard-Jones potential:

$$V_{LJ} = \frac{A}{R^{12}} - \frac{B}{R^6}, \tag{3.40}$$

where R is the distance from the structure to the hydrogen center of mass. However to get a qualitative sense of the molecular center of mass motion it is sufficient to approximate the potential as usual as a three dimensional simple harmonic oscillator. This has the familiar energy levels:

$$E_{n_x,n_y,n_z} = \left(n_x + \frac{1}{2}\right)\hbar\omega_x + \left(n_y + \frac{1}{2}\right)\hbar\omega_y + \left(n_z + \frac{1}{2}\right)\hbar\omega_z \tag{3.41}$$

From previous work in the FitzGerald group, which is consistently with current spectra, we believe that the dominating translational frequency is 84 cm^{-1} [15]. As described in Pierce's thesis [1] and in ref [2] we believe that the dominating factor in isotopologue separation is the difference in zero-point energy or lowest possible energy which occurs when all translational quantum numbers n_x, n_y, and n_z are zero. The zero-point energy (ZPE) has a $\frac{1}{\sqrt{\mu}}$ dependence where μ is the reduced mass of the molecule resulting from the frequency dependence. Thus the ZPE scales with isotopologue reduced mass. Therefore D_2 has the lowest zero-point energy and is trapped the most effectively by the MOF potential. This leads to selectivities for D_2 over H_2 in the adsorbed phase that were predicted by FitzGerald et. al. [2] and recently directly measured by Oh et. al. in the material MOF-74 [3].

3.3 Transition Intensity

In section (3.1) it was stated that infrared spectroscopy uses the interaction of light with the dipole moment of a molecule. Hydrogen being a symmetric diatomic molecule has no dipole moment in the gas phase and thus is practically invisible to infrared light.

When the hydrogen is placed into the MOF it becomes visible since the gas-MOF interaction changes the dipole moment of the system (MOF and hydrogen). This occurs through two mechanisms: the electric field from the MOF induces a dipole moment in the hydrogen, and the quadrupole moment of the hydrogen induces an extra dipole moment in the MOF atoms. The first we refer to as the polarizability mechanism, the second as the quadrupole induction mechanism. The intensity of a given transition depends on the probability of the transition (as shown in section 3.1.1). As state in Eq. 3.5 the probability depends on the mechanism that causes the induced dipole moment. These mechanisms are explored further in chapter 6.

It is important to note that in this experiment we treat all three isotopologues with the same theory. HD does possess a small inherent dipole moment but in the case of MOF-5 it appears to be negligible relative to the induced dipole moment as we do not observe any transitions associated with it.

3.3.1 Selection Rules

The selection rules of molecules in materials, which are environments with constant electric fields, differ from the infrared selection rules for free molecules. Standard infrared selection rules for diatomic molecules are:

$$\Delta\nu = \pm 1, \pm 2, ... \quad \Delta J = 0, \pm 1, \tag{3.42}$$

with $\Delta\nu = \pm 2$ and greater usually occurring with low probability [39].

However we regularly observe transitions that violate these rules, particularly pure vibrational transitions ($\Delta J = 0$), and thus must find an alternative explanation. Our observed selection rules are:

$$\Delta\nu = \pm 1, \pm 2, ... \quad \Delta J = 0, \pm 2, \tag{3.43}$$

which happen to be exactly the selection rules of the two photon Raman process in which one photon goes in and another comes out (Fig. 3.3). Condon explains this effect [40]: if the limit is taken that the frequency of one of the photons involved in Raman spectroscopy goes to zero (or the wavelength goes to ∞) a constant electric field is recovered. For the polarizability mechanism we find it useful to interpret the electric field from the MOF as a photon of infinite wavelength. It is now possible to proceed using the theory behind Raman transitions, keeping in mind that instead of an incoming photon inducing a dipole moment in the molecule the MOF's electric field does. The quadrupole mechanism does not follow the same logic. It simply causes rovibrational transitions, we do not observe a change of $\Delta J = \pm 1$ since this would require a nuclear spin to flip which is unlikely to occur in a photon transition.

3.4 Ortho and Para Hydrogen

There are two forms of molecular H_2, called ortho and para, depending on whether the spins of the protons are aligned or anti-aligned. The spins of the electrons can be neglected since they are in a 'bonding' state in molecular hydrogen with a symmetric spatial wavefunction and an antisymmetric spin wavefunction with total spin equal to zero [35]. Since protons are fermions their wavefunction must be antisymmetric under exchange, which is equivalent to a 180° rotation of the molecule. The spin of each proton is $\frac{1}{2}$ this means that the total nuclear spin quantum number is either I =1 with aligned spins or I = 0 with anti-aligned spins. The total nuclear spin forces the total

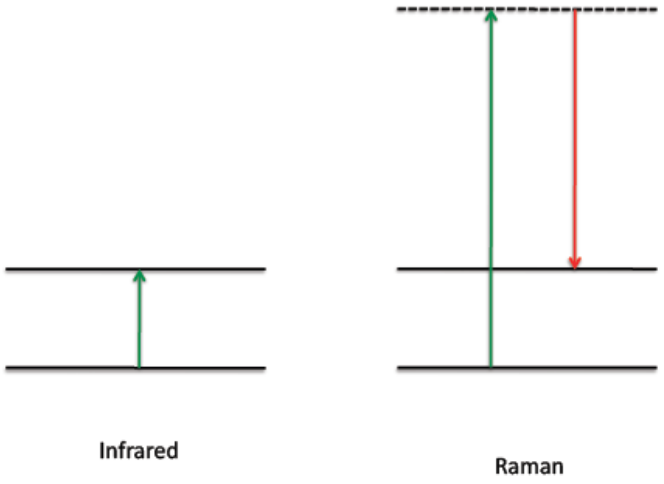

FIGURE 3.3: Schematic of difference between Raman and IR spectroscopy. In infrared one photon is either absorbed or emitted during a transition from state one to state two. In Raman one photon excites the system from state one up to some "virtual" state and then another photon is emitted as the system relaxes down to state 2. Both processes recover the information about the spacing of states one and two but with photons of very different wavelength

orbital angular momentum quantum number J to be either odd if I =1 or even if I =0 to preserve antisymmetry. Transitions caused by infrared light are dominated by effects due to the electric dipole moment and are thus unlikely to change the nuclear spin of the protons. It is possible for the magnetic dipole moment to do so but as stated in section 3.1 it is improbable to have transitions due to the magnetic dipole moment and thus they are neglected. Therefore while the true rotational ground state is J=0, I =0 many of the hydrogen molecules are trapped in the J=1, I =1 state even at low temperatures as in this experiment. However conversion is possible and as described in section 5.4 is observed in this experiment. In solid H_2 the rate of conversion is about 1.9%/hr [41], in gas phase the rate is much much slower [42]. The equilibrium ratio of ortho to para H_2 is dependent on temperature. At room temperature there is a predicted 3:1 ratio for H_2 [41], which will be the ratio exposed to the MOF-5 upon gas loading but not necessarily the initial ratio in the adsorbed phase.

Deuterium is slightly different since the nuclei are made up of a proton and a neutron the nuclear spin is 1. Thus they are bosons and must be symmetric under exchange. This causes either I = 0 with J = 1, or I = 1 with J = 0. In deuterium the equilibrium ratio at room temperature is 2:1, I = 0 to I =1 [41]. To avoid ambiguity we will not use the terms ortho and para when referring to D_2 as ortho refers to the more common species at room temperature which in D_2 is J=0. At low temperature there is still expected conversion in solid deuterium but with a smaller rate of 0.060 %/hr [41].

3.5 Population Probability

It is instructive to explore the thermal population of the different levels as a function of temperature (table 3.1). Ignoring any hydrogen-hydrogen interactions, this goes as the standard Boltzmann factor $e^{-\Delta E/k_B T}$. At our experimental temperature of 35 K we expect to only populate the ground vibrational state and very minimally populate the higher rotational and translational states.

TABLE 3.1: A comparison of transition energy to temperature, revealing what hydrogen energy levels are populated in our experimental conditions. The probability of population of an excited state is $\mathrm{P} = \mathrm{g}e^{-\Delta E/k_B T}$, where g is the degeneracy of the state. Using the experimental temperature of 35 K, ΔE is the difference between the ground and first excited state and is estimated using experimentally determined frequencies which are the same order of magnitude as in gas phase.

Transition	Frequency H_2 cm^{-1}	Temp (K)	Probability excited
Vibrational	4136	6000	10^{-74}
Rotational $J_{0\to 2}$	312	450	10^{-6}
Rotational $J_{1\to 3}$	548	790	10^{-10}
Translational	81	100	10^{-2}

Chapter 4

Experimental Procedure

4.1 Apparatus

In this experiment we used a Bomem DA3 Fourier Transform Infrared Spectrometer (FTIR) in conjunction with either a Mercury Cadmium Telluride (MCT) or an Indium Gallium Arsenide (InGaAs) detector. The sample was dosed with hydrogen using a commercially available Micromeretics physisorption analyzer. We achieved amplification of the weak signal from the hydrogen's induced dipole moment by mounting the sample in a diffuse reflectance geometry. The sample was cooled with a closed cycle helium cryostat from Janis research equipped with a home built vacuum housing to accommodate the large collecting optics. All measurements were obtained at low temperatures (below 77 K) as the hydrogen is only trapped by the MOF under these conditions. The temperature was measured with a silicone diode thermometer which was also used to give feedback to the Lakeshore 331 temperature controller.

4.1.1 The Spectrometer

Our main tool for this work, the Fourier Transform Spectrometer, is essentially a Michelson Interferometer (Fig. 4.1). It uses the principle of interference to produce a time varying signal which can be Fourier transformed to obtain an intensity spectrum as a function of frequency. A beam from a single source is divided using a CaF_2 beam splitter into two different paths. One path reflects off a stationary mirror, the other reflects off a moving mirror. The beams then recombine, interfere with each other, and pass through the sample before reaching the detector. The intensity at the detector is measured as a function of time to produce an interferogram. In the simple example of a monochromatic source when the two waves are completely in phase, the path length difference is

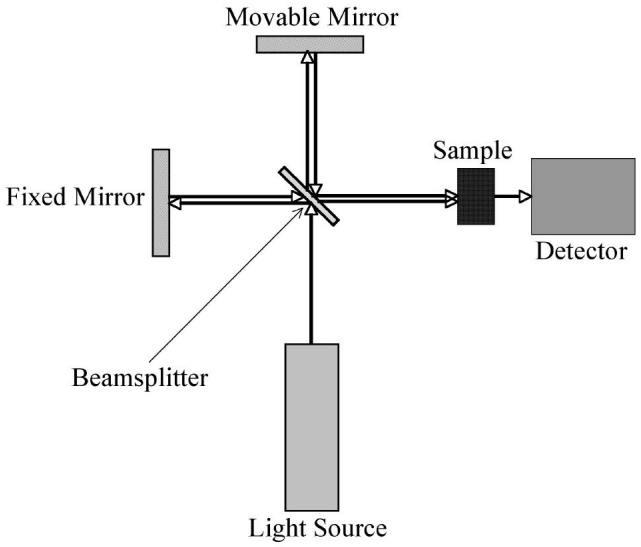

FIGURE 4.1: A schematic of a Michelson interferometer, courtesy of Simmons' thesis [43]

$\Delta L = m\lambda$, and the amplitude is twice the original amplitude. For $\Delta L = (m + 1/2)\lambda$ the beams are completely out of phase and there is complete destructive interference.

In our spectrometer we use a quartz halogen light bulb as a broadband source. The intensity at the detector is measured as a function of mirror position. Since the mirror is swept at a constant speed this is also a function of time. In our spectrometer a Helium Neon laser (with a very well known wavelength) is used to measure the movement of the mirror. A portion of the beam splitter directs the HeNe laser to a visible detector. The relative intensities of spatially separated components of the HeNe beam provide information about the angle of the stationary mirror relative to the moving one. Piezo electrics then adjust the angle of the stationary mirror to ensure that the mirrors are totally parallel to each other. For $\Delta L = 0$ all frequencies constructively interfere causing a peak in intensity at the detector. This point is detected using a visible light bulb and is the starting and ending point for each cycle of the mirror position. We obtain an interferogram by averaging over many scans or cycles of the mirror position. For maximum efficiency the mirror is slowly moved to the maximum ΔL then quickly moved back to zero path difference. The collected interferogram is then fourier transformed from a function of mirror position δ to a function of frequency ν [44]:

$$B(\bar{\nu}) = \int_{-\infty}^{+\infty} I(\delta) cos(2\pi\bar{\nu}\delta) \cdot d\delta. \tag{4.1}$$

4.1.2 Vacuum Chamber

A particular challenge of our experiment is that we must simultaneously amplify the weak infrared signal from the induced dipole moment of a hydrogen molecule, prevent the air sensitive MOFs from being exposed to atmosphere, and preform measurements at temperatures below 77 K.

Normal transmission IR spectroscopy is not ideal for studying MOF powders. The MOF grains scatter light to a large extent thus the powder can only be analyzed with transmission spectroscopy through a very thin sample which reduces the intensity of the peaks due to adsorbed hydrogen. Since scattering increases with frequency, the weak overtones are prohibitively difficult to detect using transmission spectroscopy. To solve this problem we use a technique called diffuse reflectance infrared Fourier transform spectroscopy (DRIFTS). In this technique light is focused on the sample and scatters multiple times between the MOF grains. This produces a long optical path length within the sample. The light is eventually scattered away from the sample and is collected and focused onto the detector using the DRIFTS optics (Fig. 4.2).

To perform DRIFTS measurements cold we use a modified Janis Research Company closed cycle ST-300T cryostat with a cold finger. To mount the sample within the DRIFTS collecting optics it was necessary to remove the bottom of the cryostat vacuum wall and create an external vacuum chamber. We have constructed a welded aluminum box for this purpose ($15\times12\times15$ cm^3) that houses the large collecting optics and the sample cell which is bolted to the cold finger via a copper slab. Construction of the "box" is described in detail in ref [45] and in previous theses; so only the relevant details are summarized here. Light enters and exits the box through CaF_2 windows. Figure 4.2 shows the propagation of light through the DRIFTS apparatus. The sample cell consists of a copper sample cup screwed into a copper slab. A spacer ring around the sample cup reduces the dead space volume to provide more accurate measurements of the amount of adsorbed gas. A dome with sapphire windows, transparent in the infrared encloses the sample and is bolted to the copper slab. It is sealed with indium which can operate at very low temperatures unlike rubber o-rings. A 3 mm diameter tube, soldered to the base of the sample chamber, allows us to deliver gas to the sample. Since the cryostat coldfinger contracts upon cooling we use a large plastic spacer nut to maintain the height of the sample relative to the incoming light to achieve optimal signal. The modified DRIFTS optics purchased from Spectra-Tech Inc. are bolted to the bottom of the box. Adjustable mirrors ((a) in Fig 4.3) slide aside to allow for the mounting of the sample. Temperature control is achieved using a 25 Ω heater and a silicon diode temperature sensor which are both part of the cryostat sample mount. The heater is controlled using a 331 Lakeshore Temperature controller. Another silicone diode

temperature sensor is bolted to the copper slab near the sample dome. This provides a more accurate measure of the sample temperature. The heater could be controlled using the sample thermometer but is not in order to avoid time lag oscillations.

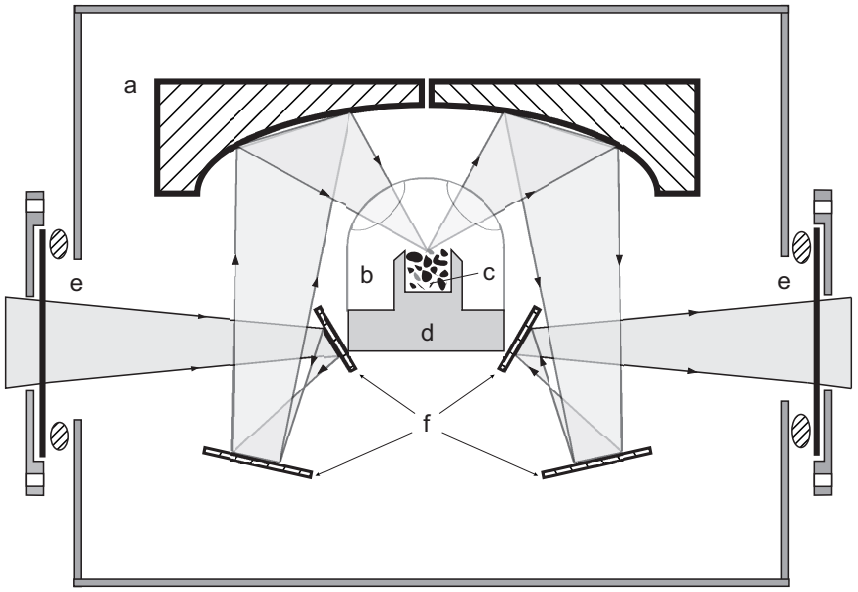

FIGURE 4.2: Schematic of radiation propagation within the DRIFTS vacuum chamber. a) Ellipsoidal mirrors, b) sample cell, c) sample powder, d) copper sample cup, e) CaF_2 windows which allow light to enter and exit, and f) plane mirrors. Courtesy of FitzGerald et. al. [45]

4.1.3 Detectors and Filters

In the collection of these data we used two semiconductor detectors. For detection over the full range of interest we used a Mercury Cadmium Telluride (MCT) detector which has a nominal optical range of 800 to 5000 cm^{-1} .While the sensitivity of the detector decreases about 5000 cm^{-1} , we were able to successfully detect peaks at frequencies as high as about 9000 cm^{-1}. We used a broad filter which blocks visible light from reaching the detector to limit the amount of noise at the detector and minimize heating of the sample. This only transmits light above about 3500 cm^{-1} so was not used to measure the fundamental D_2 peaks.

To better study the overtones we used an Indium Gallium Arsenide (InGaAs) detector with an optical range of 6350 to 11,000 cm^{-1}. Our standard procedure was to first identify the overtone peaks using the MCT detector and then employ the InGaAs detector for more detailed study. However the InGaAs is very sensitive so saturates easily. This prevents it from detecting over the whole range of the spectrum. The D* number which

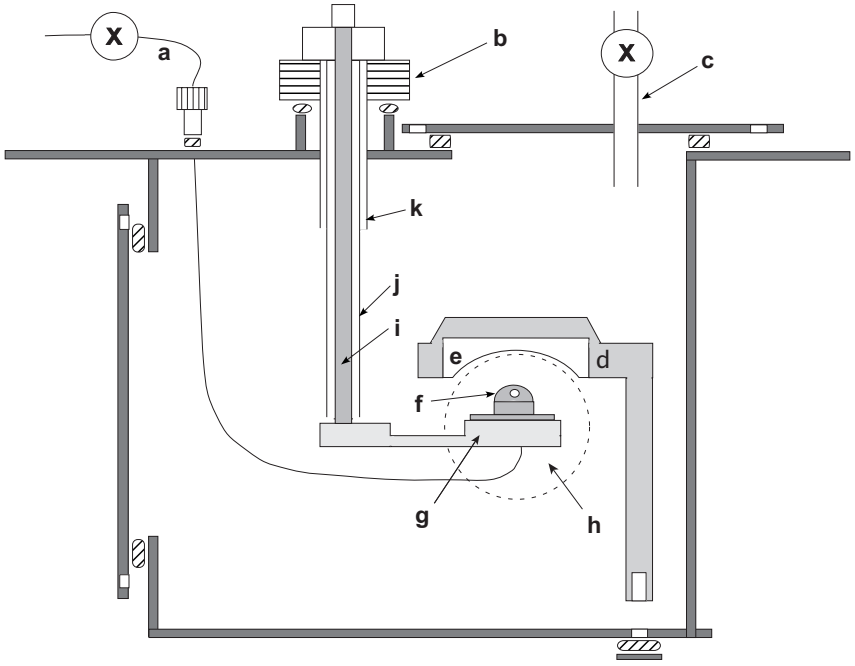

FIGURE 4.3: Schematic of the DRIFTS vacuum chamber. a) Tube to allow gas to be loaded into the sample, b) height adjustment at base of cryostat. c) evacuation line, d) mount for drifts optics, e) ellipsoidal mirror, f) sample cell holder, g) copper slab in thermal contact with cryostat and sample, h) CaF_2 window to detector, i) cold finger, j) radiation shield, and k) cutoff vacuum jacket. Courtesy of FitzGerald et. al. [45]

is a measure of relative sensitivity is 5×10^{12} for the InGaAs but only 4×10^{10} for the MCT. Thus we obtained narrow bandpass filters to limit the intensity at the InGaAs detector. We used a Thorlabs 1250 $\pm$ 2 nm (8000 $\pm$ 26 cm^{-1}) bandpass filter with a FWHM of 10 $\pm$ 2 nm (128 $\pm$ 26 cm^{-1}) to study the hydrogen vibrational overtones. Figure 4.4 illustrates the improvement in detection that is achieved with the InGaAs detector. The InGaAs achieves a resolved scan in about 1/6 of the time it takes to obtain an unresolved spectrum with the MCT detector. Future and ongoing work includes employing similar filters with different frequency ranges to measure other features such as the HD rotational overtones.

4.2 Experimental Procedure

In a standard measurement we evacuate the DRIFTS vacuum chamber using an Alcatel turbomolecular pump. This ensures that the pressure is below about 10^{-6} torr before cooling the sample in order to minimize the amount of water in the box. This minimizes ice buildup on the sample windows which produces a large infrared signal. We then cool the sample using the cryostat. We use helium as an exchange gas as it is inert and does

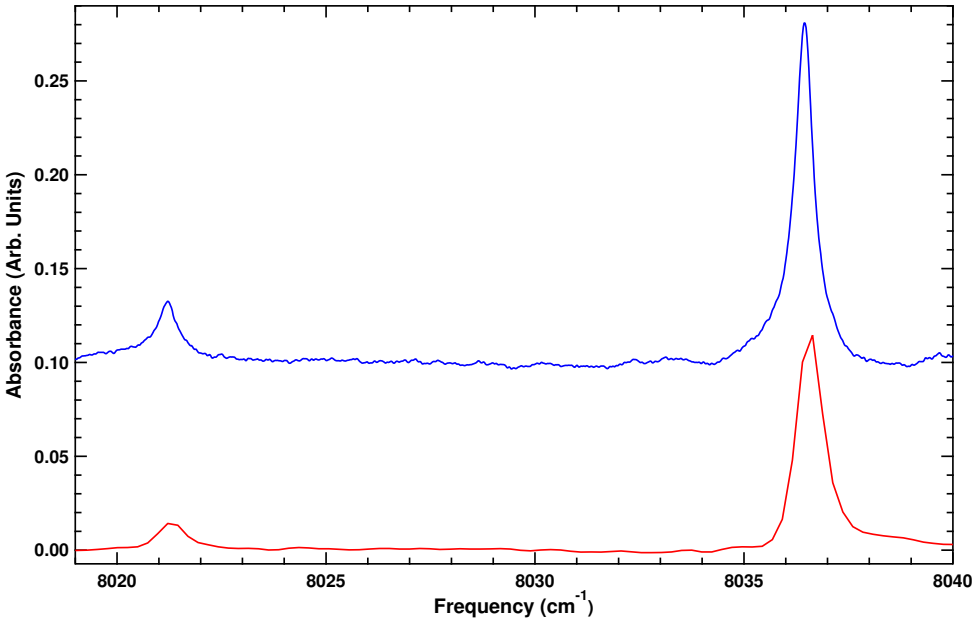

FIGURE 4.4: Comparison of spectra obtained using the MCT detector and the InGaAs detector. The InGaAs detector (blue) allows for more efficient collection of spectra due to the H_2 overtone. Both spectra are taken with a concentration of 0.9 H_2 per metal. The MCT spectrum (red) is an average of 8000 scans at 0.5 cm^{-1} resolution with a scan speed of 0.5 cm/s which takes approximately 4.5 hours to complete. The InGaAs spectrum is an average of 50 scans at 0.06 cm^{-1} resolution with a scan speed of 0.15 cm/s which takes approximately 45-60 minutes to complete. It is apparent in pointed nature of the MCT spectrum that the higher resolution is necessary to fully resolve the H_2 overtone peaks. The InGaAs achieves a resolved scan in less time than it takes to obtain an unresolved spectrum with the MCT detector.

not bind to the MOF. Its purpose is to keep the sample in thermal equilibrium. We use a commercial dosing system to add gas to the sample via the gas line. Hydrogen is either added during the cooling process or once the base temperature is achieved.

Absorbance spectra are obtained by taking a spectrum of the MOF material without any hydrogen gas loaded. The spectrum is then repeated after loading hydrogen into the MOF. The adsorbed gas contributes to a increased absorbance of light at discrete frequencies associated with the spacing of the energy levels of the molecule. By referencing the second spectrum to the first one can obtain an absorbance spectrum in which light at frequencies absorbed by the trapped hydrogen molecules are shown as peaks. This is done using the algorithm:

$$Abs = -log_{10}\left(\frac{I_s}{I_0}\right), \tag{4.2}$$

where I_s is the intensity at the detector of the scan with gas, I_0 is the intensity of the reference scan, and Abs, I_s and I_0 are all functions of frequency.

Chapter 5

Results

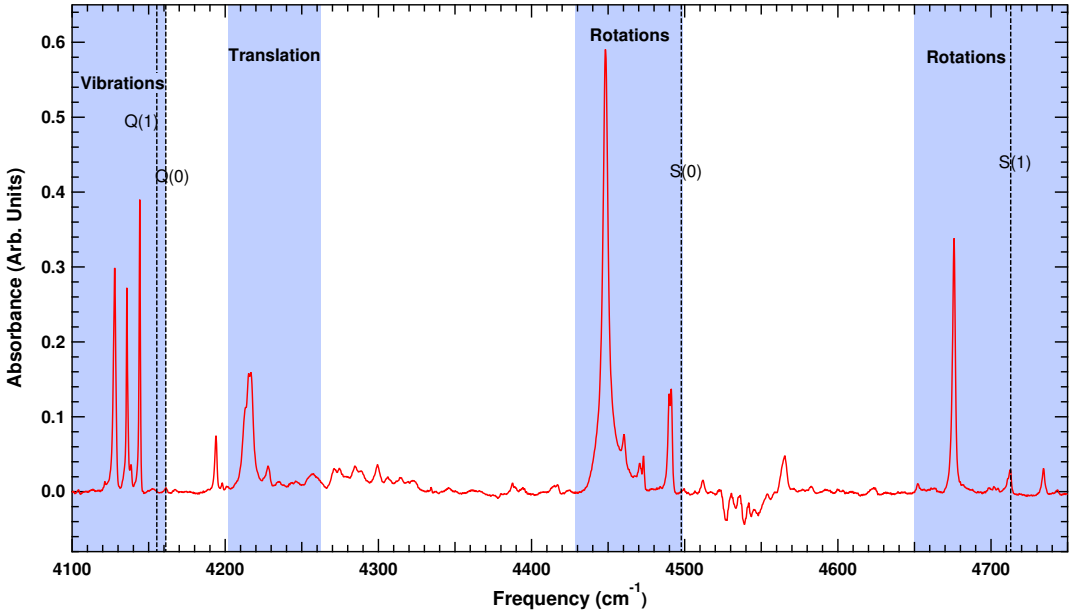

FIGURE 5.1: Absorbance spectra of hydrogen in MOF-5. The dotted black lines indicate the locations of transitions of gas phase H_2. The colored bands highlight the associated transitions of H_2 in MOF-5.

A standard absorbance spectrum of hydrogen in the fundamental region is shown in Fig. 5.1. This spectrum shows the peaks associated with the vibrations, ro-vibrational transitions, and translations of trapped hydrogen. Throughout this thesis we use the standard spectroscopic notation where Q refers to a pure vibrational transition, and S refers to a ro-vibrational transition of $\Delta J = +2$. The subscript indicates either a fundamental, $\Delta\nu = 1$, or a overtone transition $\Delta\nu = 2$. The number in parenthesis indicates the initial J quantum number. In this case (1) refers to ortho H_2 and (0) refers to para H_2 (introduced in section 3.4). By examining the spectrum of multiple isotopologues of hydrogen - H_2, HD, and D_2 - both in the fundamental and overtone

TABLE 5.1: Frequencies of the observed Q(0), Q(1), S(0), and S(1) transitions of H_2, HD and D_2. Both frequencies when free and associated with the primary, metal, binding site are shown. Transition frequencies are in cm^{-1}. The $S_1(0)$ peak of D_2 was not observed, likely due to it being obscured by the MOF-5 peaks in that region.

Isotopologue	$Q_1(0)$	$Q_1(1)$	$S_1(0)$	$S_1(1)$	$Q_2(0)$	$Q_2(1)$	$S_2(0)$	$S_2(1)$
H_2:Gas	4161.1[a]	4155.2[a]	4497.8[c]	4712.9[c]	8087[b]	8075.3[c]	8406.3[c]	8604.2[c]
H_2:MOF-5	4136	4128	4448.5 4491	4676.1 4712.1 4734.5	8036.7	8021.5	8332	8541
HD:Gas	3632.1[a]	3628.2[a]	3888[f]	4052[f]	7087[f]	7079.2[d]	7331.1[d]	7484.3[d]
HD:MOF-5	3609.6		3849		7042		7268 7280	
D_2:Gas	2993.5[a]	2991.4[a]	3166.4[e]	3278.5[e]	5868.5[b]	5863.9[e]	6034.7[e]	6140.6[e]
D_2:MOF-5	2974	2971	3127 3135		5828	5823	5980 5989	6094

a) Ref [37]
b) Ref [46]
c) Ref [23]
d) Ref [47]
e)Ref [48]
f) Calculated from Ref [37]

region we have obtained a more complete picture of the dynamics of trapped hydrogen in MOF-5 than was known previously. We have fully resolved the ortho and para peaks in the overtone for both H_2 and D_2 which gives us a powerful tool to study ortho to para conversion in both isotopologues. Table 5.1 shows the measured transition frequencies for all isotopologues when located at the primary, metal, site in MOF-5.

The advantage obtained by studying the overtone can be clearly seen in the raw spectrum of D_2 loaded in MOF-5 (Fig. 5.2) where the overtones are clear and uncomplicated by underlying MOF signal which overwhelms the D_2 transitions in the fundamental region. This power of the overtone approach is further illustrated in the rovibrational spectra of all isotopologues shown as an absorption plot relative to the pure MOF material (Fig. 5.3). Details of the rovibrational transitions will be described later. Many false peaks due to the MOF-5 not referencing out perfectly exist in the fundamental region but not in the overtone spectra.

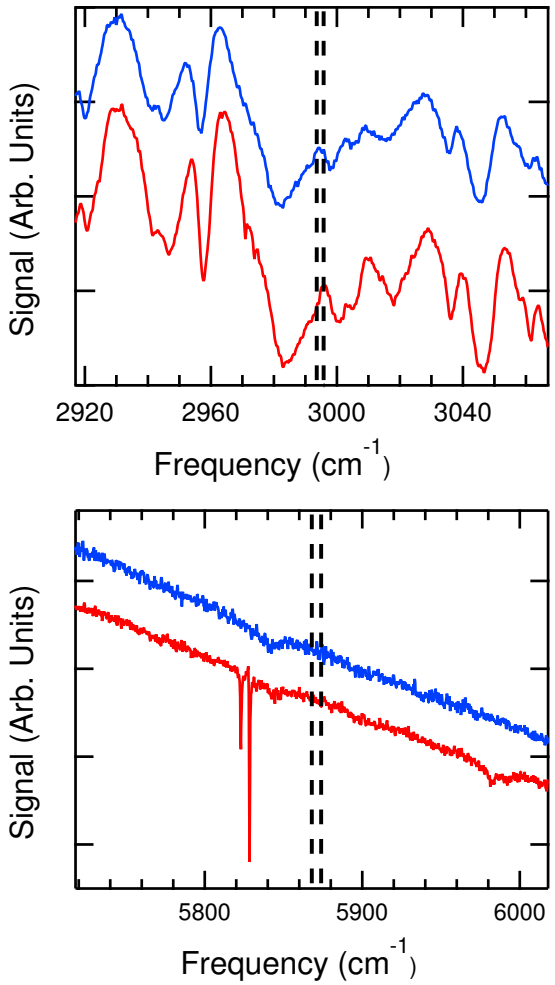

FIGURE 5.2: Raw spectrum of MOF-5 without gas loaded (blue) and after being loaded to a concentration of about 0.7 D_2/Zn (red). The dotted lines indicate the gas phase Q(1) and Q(0) transitions. The deuterium peaks in the fundamental region (top) are weak compared to the MOF-5 peaks and thus difficult to interpret. In contrast the peaks in the overtone region (bottom) are clear. The overtone and fundamental regions shown in the separate panels display different parts of the same experimental spectrum. Therefore it is guaranteed that all experimental conditions including temperature, concentration, and ortho to para ratio are the same in both regions.

5.1 Isotopic Substitution

In Buckingham's influential paper [49] he used up to second order perturbation theory to show that when diatomic molecules are trapped in materials the shift of the transition frequencies from gas phase divided by the molecular constant ω_e is approximately constant upon isotopic substitution:

$$\Delta f/f \approx \Delta\omega/\omega_e = \text{constant}. \tag{5.1}$$

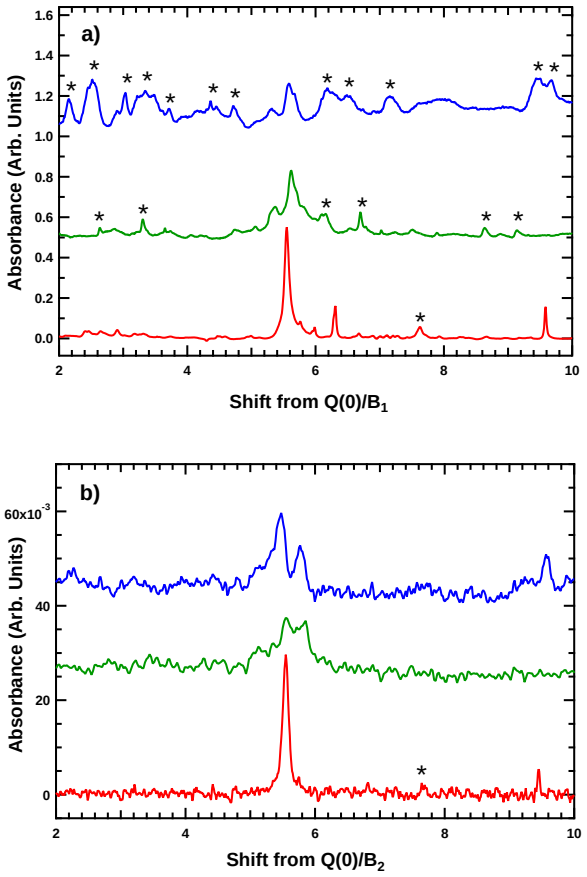

FIGURE 5.3: Rotational peaks of all isotopologues, a) shows the fundamental region, b) shows the overtone. The D_2 (blue) spectrum is at a concentration of 0.7 D_2/Zn; HD (green) is at a concentration of 0.7 HD/Zn in the fundamental and 0.9 HD/Zn in the overtone, H_2 (red) is at a concentration of 0.9 H_2/Zn. The slight concentration difference does not produce significant changes in the spectra as at both concentrations the metal site is not saturated. For H_2 the two panels show different portions of the same spectra so there is no experimental difference between the overtone and fundamental. The spectra for the other isotopes were chosen as the ones that best resolve the overtone peaks. All spectra are scaled so that the S(0) peak coincides for all isotopologues both in the overtone and fundamental. As these peaks are due to a ro-vibrational transition with $\Delta J = +2$ we have plotted the shift from the pure vibrational transition Q(0) and scaled all transitions by the appropriate rotational constant. B is the rotational constant which as described in section 3.2.2.1 varies depending on isotope and vibrational state, indicated by the subscript. As described in section 3.2.2 the S(0) peaks should be about BJ(J+1) above the Q(0) peaks. The HD and D_2 spectra are scaled by two in the overtone in order to display them alongside the more intense H_2 peak. Stars indicate areas where the MOF-5 background spectrum did not correctly cancel out.

Because $\omega_e \approx f$ where f is the gas phase transition frequency $\Delta f/f$ is also approximately constant.

The molecular constant ω_e is determined through spectroscopic measurements and is well known for all isotopologues of hydrogen. For H_2 it is 4400.39 [37] cm^{-1}, for HD it is 3881.92 cm^{-1} [37], and for D_2 it is 3115.5 cm^{-1} [22]. There is a slight spread in the

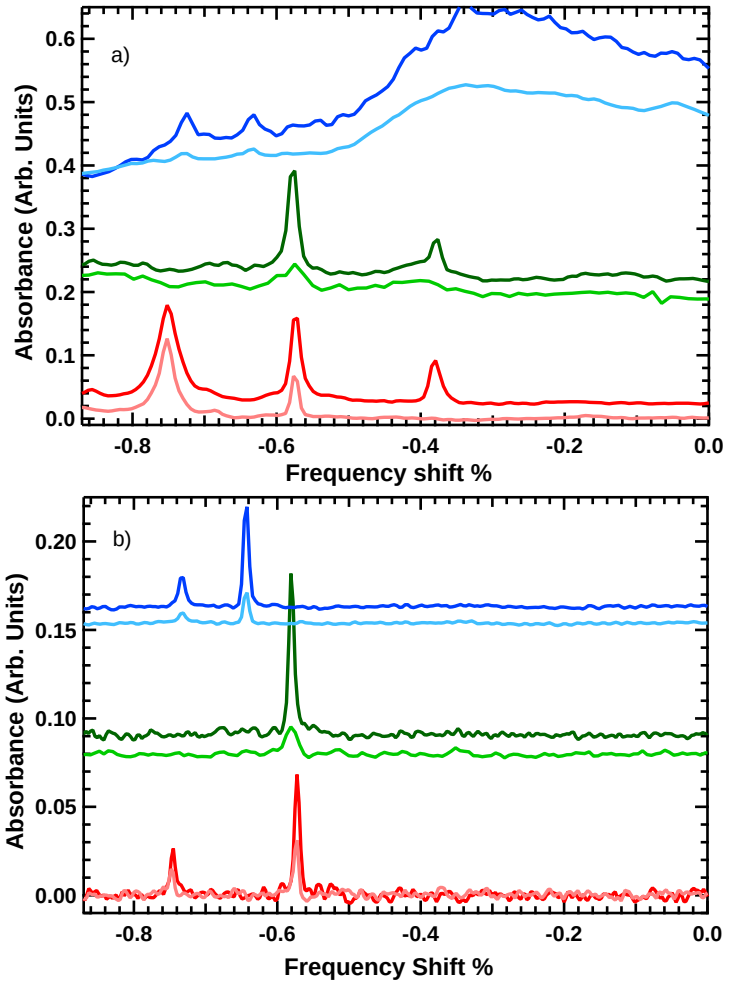

FIGURE 5.4: Vibrational bands of all three isotopologues: D_2 (blue), HD (green), and H_2 (red). a) Shows the fundamental transitions. b) Shows the overtone region. For H_2 and D_2 both the ortho and para vibrational peaks are apparent (Q(0) and Q(1)). The frequency axis which displays redshift from the gas phase Q(0) frequency has been scaled by $1/\omega_e$, where ω_e is the molecular constant, so as to demonstrate the agreement with the Buckingham theory. The location of vibrational lines are very sensitive to the chosen gas phase frequencies which values vary slightly in the literature. Those used here are from table 5.1. All isotopologues line up and the overtone and fundamental region line up. Spectra are shown at concentrations of 0.2 (light) and 0.7 (dark) hydrogens per metal. The two panels show different portions of the same spectra with the exception of the 0.7 hydrogen/Zn concentration D_2 overtone for which a broadband filter (described in section 4.1.3) was used. Spectra are offset for clarity.

literature values. Thus the reference that seemed to be most widely accepted was used for Fig. 5.4. This constant ω_e is the frequency associated with the simple harmonic term in the Hamiltonian describing the trapped molecule [49] and thus scales as $1/\sqrt{\mu}$, where μ is the reduced mass of the isotopologue being studied. Buckingham also showed that the shift from gas phase should be double in the overtone:

$$\Delta\omega_{n\leftarrow 0} = n\Delta\omega, \tag{5.2}$$

where n is the nth vibrational level, in our case n = 2. These facts allow us to plot the vibrational spectra so that both the fundamental and overtone transitions for all isotopologues can be considered simultaneously (Fig. 5.4). The fundamental region is scaled by $\frac{1}{\omega_e}$ and the overtone region is scaled by $\frac{1}{2\omega_e}$. Buckingham's theory predicts a perfect overlap of all peaks due to the same transition. Deviations of the isotopologues from perfect alignment, within 0.1 %, most likely reflects the fact that the MOF-gas interaction is averaged over the center of mass translational ground state wavefunction of the adsorbed isotopologue. It is interesting to note that H_2, HD and D_2 are progressively more shifted. The difference between the D_2 and HD shift is greater than the difference between the HD and H_2 shift. This could be an artifact of the gas phase frequencies used to compute shift as they vary somewhat in the literature however the same behavior is seen in the vibrational spectra of all isotopologues in the material know as MOF-74 [50]. Failure of peaks associated with the same isotopologue to line up in the fundamental versus overtone region is due to modification of the anharmonicity of the molecule in the excited state. This is a deviation from the Buckingham model which assumes that the anharmonicity is constant. While there are some deviations from perfect alignment in Fig. 5.4 the peaks line up fairly well which is an indication that Buckingham's theory is applicable here. The line locations closely follow what is expected from Buckingham's theory but as we will show in chapter 6 the line intensities do not.

5.2 Redshift

One of the advantages of studying MOF-5 is that the different crystallographic binding sites have been well established using low temperature diffraction experiments as described in chapter 2. In the next sections we outline our procedure for assigning the different infrared features to hydrogen at the different crystallographic sites, building on previous work in the FitzGerald group [15]. It has been seen in multiple materials including MOF-74 [51] and MOF-5 [15] that redshift of the vibrational peaks from gas phase correlates with binding energy of the site (Fig. 5.5). Thus as a general rule the most redshifted vibrational peak corresponds to hydrogen at the site with the greatest binding energy.

5.3 Concentration Dependent Spectra

In order to further identify which peaks are due to which binding sites in the MOF we examine hydrogen spectra as a function of concentration or number of H_2 per metal site. We know that at low concentration thermodynamics predicts that for a system

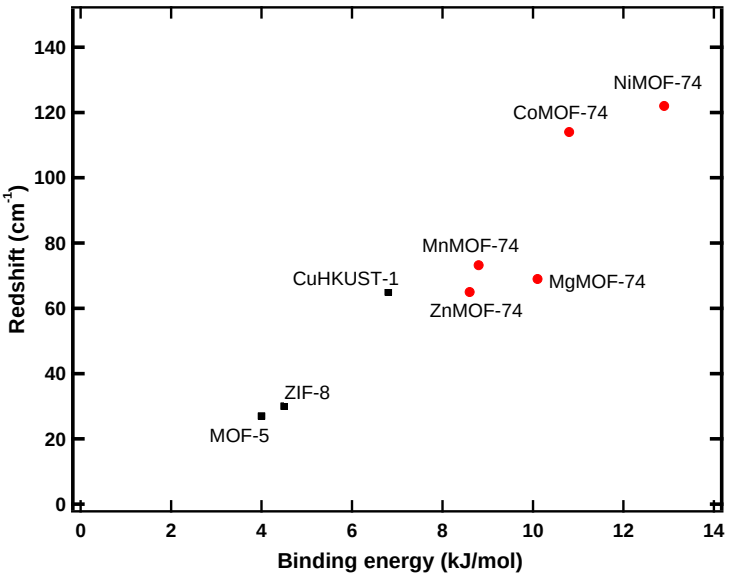

FIGURE 5.5: Redshift versus binding energy (kJ/mol) for a variety of materials, demonstrating the experimentally observed correlation.

with only two possible sites and equal degeneracy the relative population is given by $e^{-\Delta E/k_B T}$. Thus at low enough temperature almost all of the observed transitions arise from hydrogen at the crystallographic site with the greatest binding energy. This becomes more complicated for a realistic system such as ours with multiple distinct crystallographic sites. However, because all sites have comparable degeneracy, at low temperature and low concentration the most intense peaks arise from hydrogen at the highest binding energy site which in MOF-5 is known to be the metal site. Our previous infrared measurements have estimated a binding energy of 4 kJ/mol for the metal site and 2.5 or 3 kJ/mol for the various secondary sites [15]. Thus since ΔE is approximately 1-2 kJ/mol for the primary metal site relative to any of the other sites the relative concentration is predicted to be about 0.03 at 35 K - most of the hydrogen occupies the metal site. The ability to distinguish between different sites is a powerful feature of spectroscopy and is important because the metal site is often of most interest for practical purposes. As shown in Fig. 5.6, in the fundamental region new peaks appear as a function of concentration as the multiple secondary sites in the MOF are populated. In the overtone region however the two visible peaks grow but no new ones appear until the very high concentration of 3 H_2/Zn. The peaks due to H_2 at the secondary sites are much weaker in the overtone even at concentrations well above the saturation level for the primary site (Fig. 5.7); H_2 molecules at the metal site are amplified in the overtone region. This is useful for the study of the metal site and indicates that H_2 at the metal site has an interesting, different behavior. The frequency range in Fig. 5.6 extends as far as the gas phase value for both the fundamental and overtone - this is sufficient to

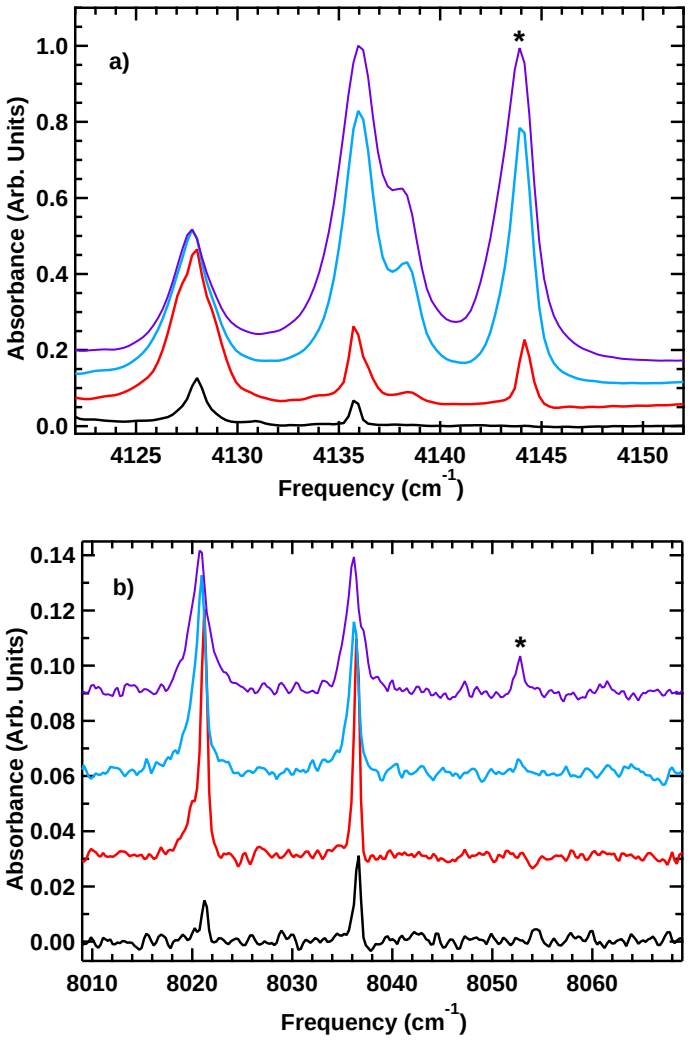

FIGURE 5.6: Vibrational Spectra of adsorbed hydrogen at various concentrations in MOF-5 for 0.2 (black), 0.9 (red), 2 (blue), and 3 (purple) H_2 /metal, demonstrating the amplification of the H_2 at the metal site in the overtone. a) The fundamental region shows peaks associated with secondary and tertiary sites appearing at higher concentrations. b) The peaks due to H_2 at the secondary site are only visible at very high loading in the overtone and are greatly reduced relative to in the fundamental where the secondary peaks dominate. The stars indicate the secondary peak whose corresponding peak is visible in the overtone. The two panels show different portions of the same spectra

show all vibrational peaks since frequencies for all known adsorbed hydrogen peaks are redshifted relative to the gas phase.

5.4 Ortho to Para Conversion

As introduction in section 3.4 ortho to para conversion is expected to occur in solid H_2 at a slow rate of 1.9%/hr [41]. In gaseous hydrogen it is expected to occur at an

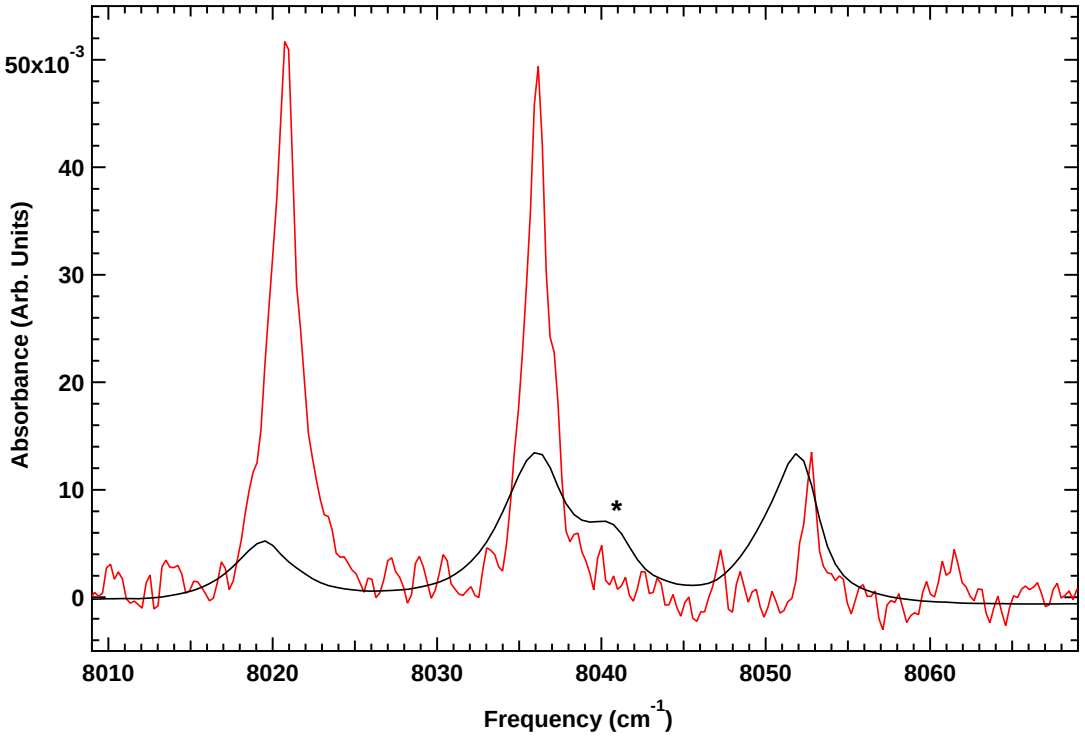

FIGURE 5.7: Vibrational Spectra of adsorbed H_2 in MOF-5 that demonstrates that the intensity of the peaks due to H_2 at the secondary sites is decreased in the overtone. Concentration of 3 H_2 per metal site binding site. The spectrum from the fundamental region (black) has been plotted in the overtone region (red) with the frequency axis stretched by a factor of two and the y axis scaled by a factor of 1/60. The intensity in the overtone of the secondary Q(0) peak at 8052 $cm^{-1}$is 1/(125±20) of the intensity in the fundamental. This is in contrast to the primary Q(0) which is only down by a factor of 1/2.5 and the primary Q(1) which is down by a factor of 1/14. The feature indicated by the star is a secondary Q(1) peak in the fundamental and is not evident in the overtone. This demonstrates how suppressed the secondary peaks are relative to the primary. This is very different from the fundamental region where the secondary peaks are of the same order of magnitude as the primary.

extremely slow rate [52]. However we observed conversion occurring on the order of minutes when exposing hydrogen gas to a cold MOF-5 sample (30-40K). By keeping the temperature constant and observing change in the spectra over time we have analyzed this conversion. Ortho to para conversion is both interesting in its own right and allows us to identify the origin of peaks by observing which ones change as a function of time when temperature and concentration are held constant. This tells us whether the peaks are associated with an initial J=0 or J=1 quantum number as the first is expected to grow with time and the second is expected to decrease. We initially measured the conversion using the MCT detector (Fig. 5.8). However as described in section 4.1.3, due to its lack of sensitivity the MCT requires a long averaging time to obtain a sufficient signal to noise ratio. This is not ideal to study the rapidly changing conversion phenomena. Thus we repeated the experiment with the InGaAs detector which as

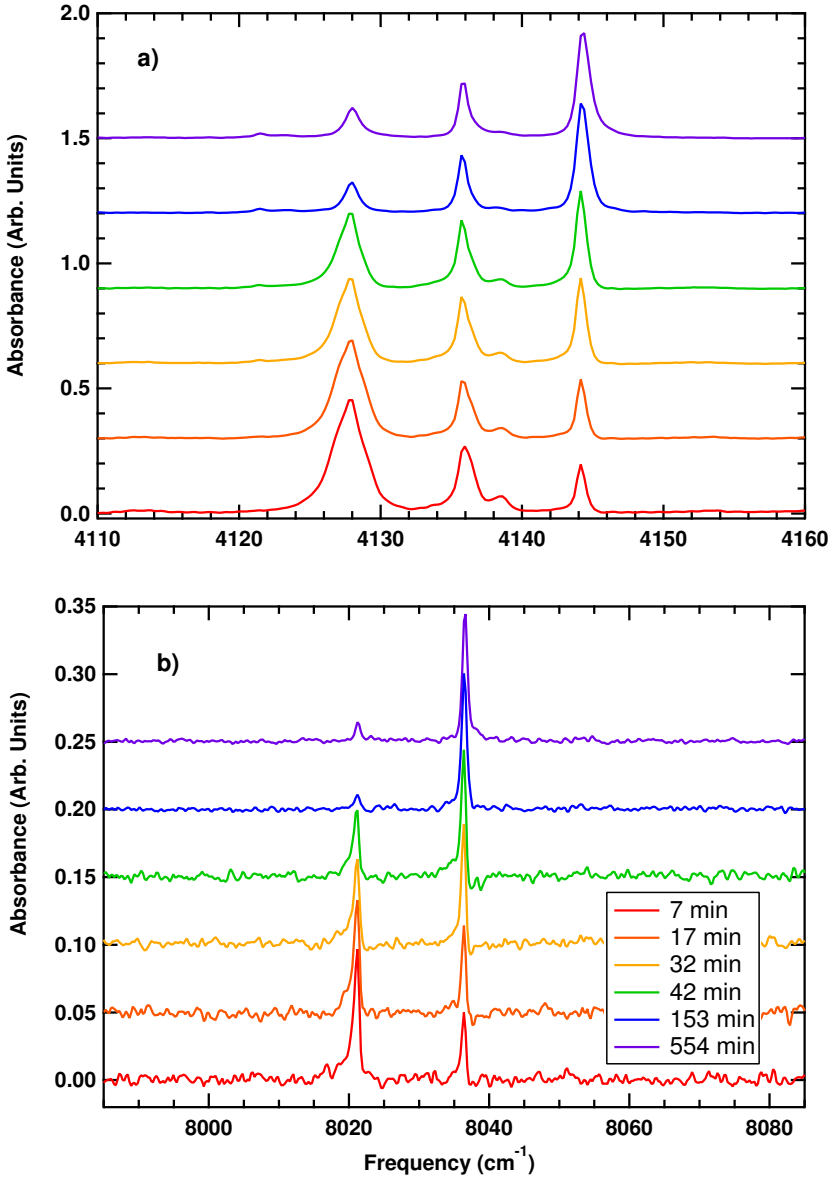

FIGURE 5.8: Ortho to Para Conversion Spectra taken using MCT detector. MOF-5 loaded with a concentration of 0.9 H_2 /metal and a temperature of 37-39 K. a) Shows the fundamental region. The far right peak is due to hydrogen at the secondary site. b) Shows the overtone region; it is clear that initially most of the hydrogen is in the ortho (J=1) state (red) and that after conversion has taken place most of it is in the para (J=0) state (purple). The two panels show different portions of the same spectra. Thus spectra taken at each point in time are experimentally identical.

described in section 4.1.3 is about 100 times more sensitive than the MCT (Fig. 5.9). This allowed us to obtain data earlier in the conversion process. We determined the number of ortho H_2 to para H_2 as a function of time using a multi step process. First the peaks are each fitted to a single voigt function, which is a convolution of a lorentzian and a gaussian. However the area of the peaks corresponds to the number of hydrogens molecules times the relevant dipole moment. To determine the dipole moment for the

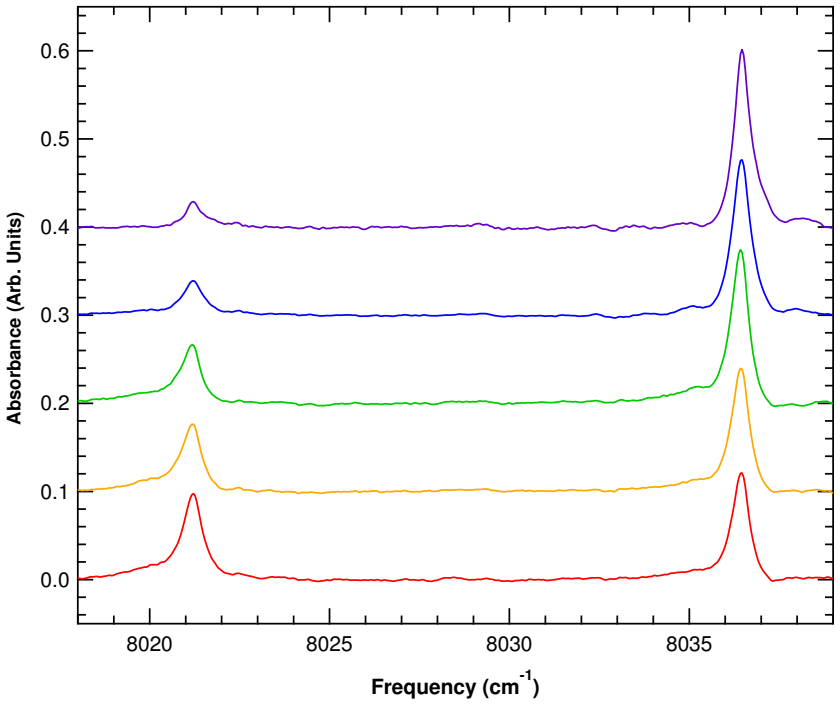

FIGURE 5.9: Ortho to Para Conversion Spectra taken using InGaAs detector. MOF-5 loaded with a concentration of approximately 0.9 H_2 /metal, and a temperature of 40-42 K. The spectra of H_2 in the overtone region are taken with the InGaAs detector and a resolution of 0.25 cm^{-1}.

$Q_2(0)$ and $Q_2(1)$ transitions we took the ratio of two spectra taken at different times in the conversion process. By comparing a spectra to one taken earlier in the conversion process we produced a difference spectra (Fig. 5.10). This has an upward-going peak due to an increased para H_2 concentration, and a downward peak due to decreasing ortho H_2 concentration. Under the assumption that no changes in the system of adsorbed concentration or temperature occurred during this time we are assured that each peak corresponds to the same number of molecules and thus the relative intensity is indicative of the dipole moment. Thus we believe that the dip at 8021 cm^{-1} and the peak at 8036 cm^{-1} are caused by the same number of molecules. Now we can convert the relative intensity of the Q(0) and Q(1) peaks into a relative number of ortho and para H_2 and thus plot the ratio in the adsorbed phase as a function of time (Fig. 5.11). The conversion we have observed in MOF-5 and in other materials including Zn-MOF-74 [51, 53] was surprising as there are no inhomogeneous magnetic fields in Zn based MOFs which would be the standard explanation for an increased rate of ortho to para conversion of molecular hydrogen in the adsorbed phase. Conversion does occur in the magnetic versions of MOF-74 at a much faster rate [53]. Within the past year there has been theoretical work done to explain conversion processes in non magnetic materials where conversion is proposed to occur through "Fermi" contact interaction or non zero

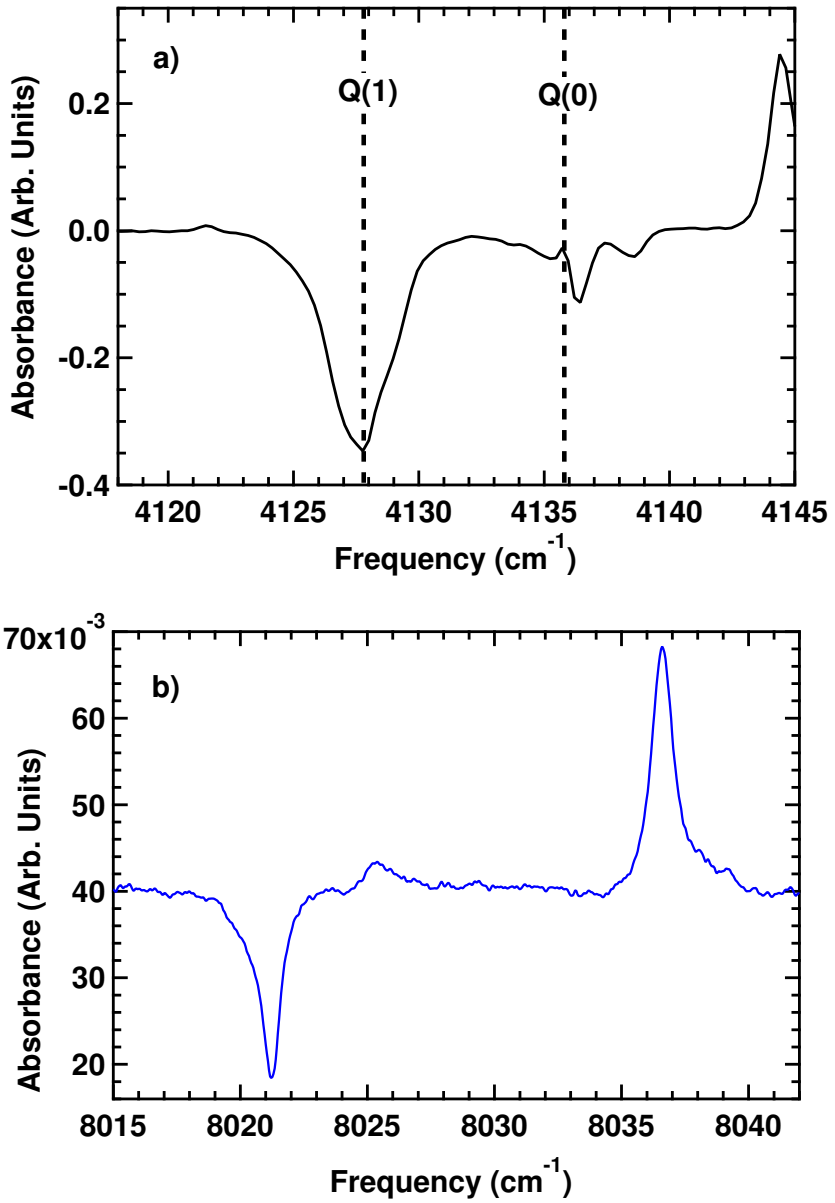

FIGURE 5.10: Relative absorbance of ortho and para hydrogen. a) The fundamental region taken with the MCT detector at a resolution of 0.5 cm^{-1} and a concentration of 0.9 H_2/metal. The fundamental region is ill suited for the goal of establishing the dipole moment of adsorbed hydrogen as the secondary and primary peaks overlap. b) The overtone region taken with the InGaAs detector, a concentration of 0.9 H_2 /metal, and a resolution of .125 cm^{-1}. Analysis of the overtone spectrum is used to determine the intensity caused by the same number of molecules in the ortho and para states.

probability of electron density occurring at the hydrogen nucleus which leads to a faster rate of conversion than previously envisioned for this type of material [42, 54]. In this case angular momentum is conserved by the flipping of an electron spin on the MOF leading to the flipping of a nuclear spin on the hydrogen.

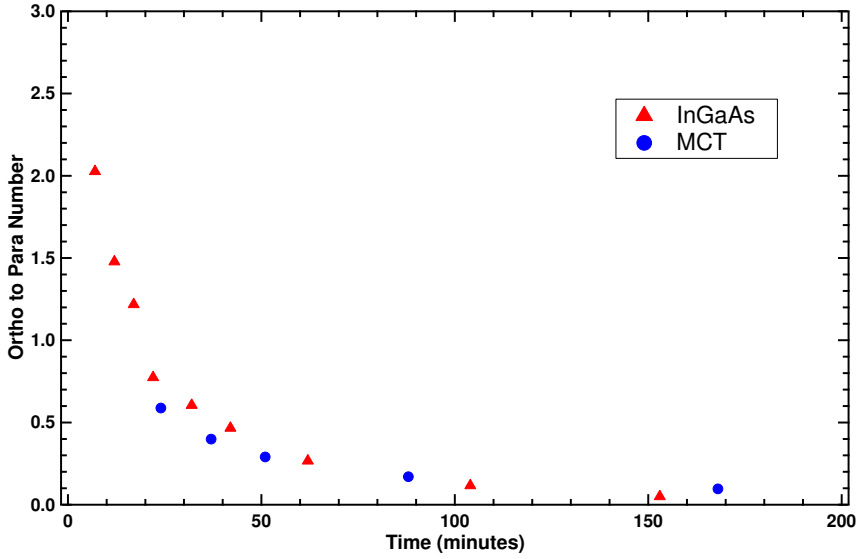

FIGURE 5.11: Rate of Ortho to Para Conversion: the number of ortho and para H_2 are calibrated relative to intensity using methods described in Fig. 5.10. The ortho/para intensity ratio is scaled by 0.6±0.1 to arrive at the ortho to para number ratio. The InGaAs detector allows for faster collection of data, thus earlier measurements of the conversion rate.

5.5 Overtone Width

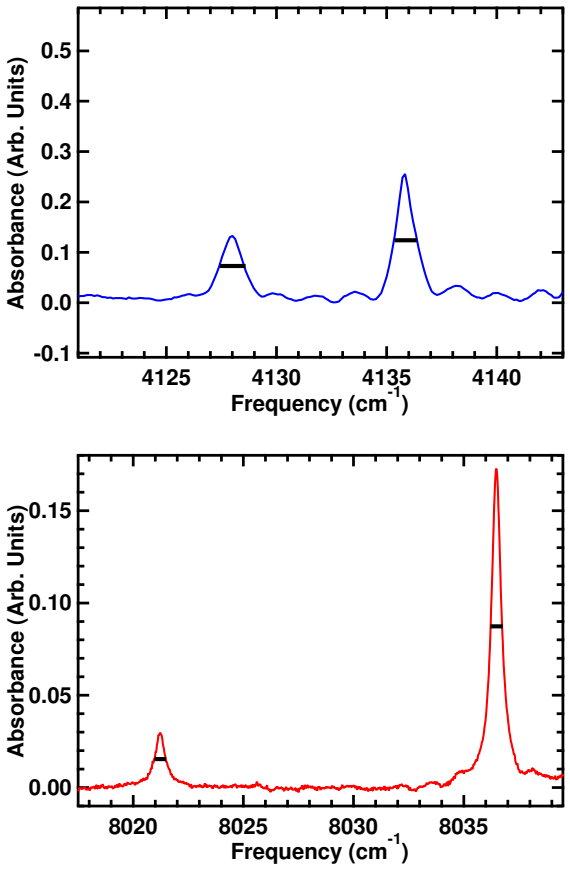

FIGURE 5.12: Spectra of overtone and fundamental which shows sharpness of H_2 overtone in MOF-5 with a concentration of about 0.9 H_2 per metal, showing overtone (bottom) and fundamental regions (top) on the same scale but taken with different detectors. The fundamental spectra is taken with the MCT detector and a resolution of 0.25 cm^{-1}. The overtone spectra is taken with the InGaAs detector at a resolution of 0.06 cm^{-1}. Both graphs have the same range of frequencies to assist in the comparison of peak width. The FWHM is shown as black bars on all spectra.

Figure 5.12 shows a comparison between the overtone and fundamental regions on the same frequency scale. The top spectrum shows fundamental region, spectrum taken with a resolution of 0.25 cm^{-1} at 38 K with the MCT detector. When fitted to a mixed gaussian and lorentzian profile the fundamental Q(0) peak was 99% lorentzian, the Q(1) displayed a lower percentage of lorentzian. The absence of a good fit for the Q(1) fundamental is likely due to overlap with secondary peaks. The bottom spectrum shows overtone region, spectrum taken with a resolution of 0.06 cm^{-1} at 43 K with InGaAs detector. Both graphs show frequency ranges of 22 cm^{-1}. The frequency axis has not been scaled. This demonstrates the sharp character of the overtone transition beyond the fact that the resolution used for the overtones is higher. The full width at half max (FWHM) for the overtone is 0.56 and 0.53 for the Q(1) and Q(0) respectively

while it is 1.1 and 1.0 for the fundamental. Both scans were Fourier transformed using the Boxcar apodization which results in higher resolution than the Bartlett apodization which is used in all other spectra. The sharp character of the overtone is indicative of a large lifetime of the excited state based on the energy, time uncertainty principle $\Delta E \Delta t \geq \hbar/2$. The apparent slow relaxation time from the $\nu = 2$ state indicates that H_2 coupling to the MOF is slower at these frequencies. When fit to a mixed gaussian lorentzian profile the overtone peaks were primary lorentzian in shape, at least 70 % percent, though they varied somewhat depending on the resolution. This indicates a lifetime limited peak width and not an inhomogeneous broadening. This is consistent with the results from the fundamental region. Inhomogeneous broadening, caused by different molecules experiencing slightly different environments throughout the material, would result in the overtones having twice the width of the fundamental [49].

Chapter 6

Analysis

Here we continue the discussion of the nature of the induced dipole moment and the two mechanisms which cause it. The nature of the dipole moment directly impacts the intensity of peaks in the spectrum of adsorbed hydrogen, as shown in section 3.1.1. This particularly effects the relative intensity or probability of observing various transitions.

When the hydrogen is adsorbed into the MOF it becomes infrared active since hydrogen transitions change the dipole moment of the system through gas-MOF interactions. This occurs through two mechanisms. The first is the polarizability mechanism in which the electric field from the MOF induces a dipole moment in the hydrogen, separating the charge and making the hydrogen visible or able to absorb incident light. The second mechanism is the quadrupole induction mechanism in which the permanent quadrupole moment of the hydrogen induces an additional dipole moment in the MOF atoms upon hydrogen being adsorbed. While gas phase hydrogen also has a quadrupole moment, any affect caused by free hydrogen is broadened out due to the brief interaction time and falls off with a one over distance to the fourth power, thus is not significant for our spectrum. The induced dipole moment caused by the polarizability mechanism is:

$$\vec{\mu}_{ind,pol} = \alpha_{H_2} \cdot \vec{E}_{MOF}, \tag{6.1}$$

where α_{H_2} is the polarizability tensor of the hydrogen molecule and E_{MOF} is the electric field from the MOF. In principal α_{H_2} is a function of θ and ϕ. However as we will show the anisotropic component of α_{H_2} is negligible. Polarizability is a measure of how easily an electric field creates a separation of charge. The induced dipole moment caused by the quadrupole induction mechanism at each point in the framework is:

$$\vec{\mu}_{ind,MOF} = \alpha_{MOF} \cdot \vec{E}_{quad}, \tag{6.2}$$

where α_{MOF} is the polarizability of the MOF, and is not uniform over the whole framework since it depends on the specific atoms. The electric field from the permanent quadrupole moment of the hydrogen is $\vec{E}_{quad} = Q_{H_2}(\theta, \phi)/R^4$, where Q_{H_2} is the quadrupole moment of the hydrogen molecule and the θ and ϕ dependence reflect the fact that the direction of the quadrupole field depends on the orientation of the hydrogen molecule. $\vec{E}_{quad}$ interacts with this polarizability of the MOF to induce dipoles in the MOF structure. Here R is the distance from the hydrogen center of mass to a point on the structure. To get the total induced dipole moment from the quadrupole mechanism we sum over the whole structure.

$$\vec{\mu}_{ind,quad} = \sum_{MOF} Q_{H_2}(\theta, \phi) \frac{\alpha_{MOF}}{R^4}. \tag{6.3}$$

This term could in principle be calculated by performing a sum over the framework. However that would require knowing the exact polarizability at each point and is presently intractable. It is important to note that while we know the R dependence of the quadrupole electric field at each point we do not know the R dependence of $\mu_{ind,quad}$ since calculating it involves a vector sum. In the extreme one could imagine situations in which due to symmetry there was no induced dipole moment.

The total change in the dipole moment of the system which is responsible for the peaks in the absorption spectra is defined as:

$$\vec{\mu}_{sys} = \vec{\mu}_{ind,pol} + \vec{\mu}_{ind,quad}. \tag{6.4}$$

We do not know the relative magnitude of each term, however it is useful to rewrite Eq. 6.4 as:

$$\vec{\mu}_{sys} = C\alpha_{H_2} + DQ_{H_2}(\theta, \phi), \tag{6.5}$$

where C depends on the MOF electric field and D depends on the sum over the MOF but both are approximately constant over the hydrogen molecule when it sits at a potential minimum at a binding site.

6.1 Transitions and Mechanisms

In the following sections we explore which transitions are due to what mechanism (table 6.1) and how this changes in the overtone. Here we outline the dependence. We justify our statements in sections 6.2-6.3. Comparing the origin of various transitions can give us insight into the hydrogen molecules' behavior and help us understand our spectra (Fig. 6.1). The pure vibrational transition in the ground rotational state, Q(0), is purely due

TABLE 6.1: Peaks and summary of the contributions from polarizability mechanism and quadrupole induction mechanisms.

	$Q(0)$	$S(0)$	$Q(1)$	$S(1)$
Polarizability Mechanism	Yes	No	Yes	No
Quadrupole Induction Mechanism	No	Yes	Yes	Yes

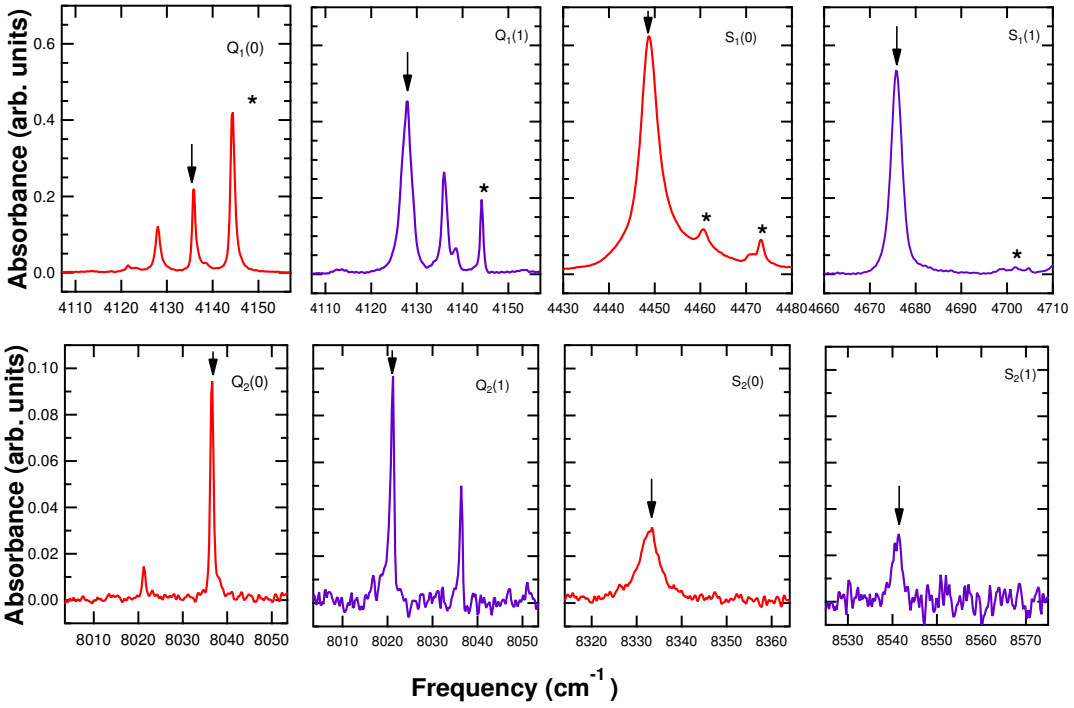

FIGURE 6.1: The Q and S bands for the fundamental and overtone region. This illustrates the change in the relative intensity between fundamental and overtone. The frequency window on horizontal axis is the same for all panels. Top shows fundamental peaks; bottom shows corresponding overtone peaks. All spectra are taken with MCT detector with hydrogen loaded to a concentration of approximately 0.9 H_2/metal at 40 K and a resolution of 0.5 cm^{-1}. The purple spectra are initial data before much conversion has taken place, red shows data after conversion has caused the ortho to para ratio to come to close to its final value. The stars indicate peaks associated with secondary sites. The arrows indicate the peak for which each panel is labeled.

to the polarizability mechanism. This is because the J=0 state is spherically symmetric, so has no quadrupole moment. The S peak transitions which involve a change in the rotational, J quantum number, are caused by the quadrupole induction mechanism. The polarizability mechanism is largely isotropic and therefore contributes negligibly. The Q(1) pure vibrational transition with J=1 is caused by both mechanisms. Thus it is interesting but challenging to examine theoretically.

Figure 6.1 demonstrates that while the Q peaks become much sharper in the overtone, as described in section 5.5, the S peaks do not. The S peak width is dependent on

the lifetime in the excited state which is due to the relaxation from J=2 to J=0 or J =3 to J=1 due to coupling to a MOF phonon which does not depend significantly on the vibrational state. Again neither the Q or S peaks experience the inhomogeneous broadening predicted by Buckingham (described in section 5.5). Both the S and Q peaks in the overtones when fit to a mixed Gaussian and Lorentzian line profile are at least 70% Lorentzian. This further supports the lack of inhomogeneous broadening which would tend to result in a Gaussian profile [55].

6.2 Pure vibrational Q(0) transition

When examining the Q(0) pure vibrational transition we only consider the polarizability mechanism. The J=0 state is spherically symmetric and thus has no quadrupole moment. The predicted intensity of transitions, which is proportional to $|\langle\psi_i|\mu_{sys}|\psi_f\rangle|^2$, should follow the exact same form (except for a frequency prefactor) as the predicted line intensities in raman spectroscopy [43, 56], given by Ref [57]. This can be understood using the same reasoning as in section 3.3.1: the electric field acts like a photon with infinite wavelength. Thus the physical process of an infrared photon exciting a transition is completely analogous to the two photon process used in Raman spectroscopy. We can make sense of the Q(0) transition purely by following theory [58, 59], and experiment [21, 22, 37] for Raman transitions in gas phase hydrogen. Our ultimate goal is to explain our observed relative intensity of hydrogen in the fundamental versus the overtone.

We follow the theory presented in Knippers et. al. for homonuclear diatomic molecules [22]. While HD is not a homonuclear molecule its electronic wavefunction is almost exactly the same as in H_2 and D_2 thus it follows the same theory to a good approximation. The polarizability is given as a tensor; in the frame where the Z axis is parallel to the hydrogen molecular axis it is:

$$\alpha_{X'Y'Z'} = \begin{pmatrix} \alpha_{\parallel} & 0 & 0 \\ 0 & \alpha_{\perp} & 0 \\ 0 & 0 & \alpha_{\perp} \end{pmatrix}. \tag{6.6}$$

It is traditionally described in terms of an isotropic part $\bar{\alpha}$ which does not depend on angular coordinates θ and ϕ, and an anisotropic part γ which does:

$$\bar{\alpha} = \frac{1}{3}(\alpha_{\parallel} + 2\alpha_{\perp}), \tag{6.7}$$

$$\gamma = \alpha_{\parallel} - \alpha_{\perp}. \tag{6.8}$$

The polarizability is written as an expansion in the dimensionless quantity ξ (Eq. 3.26) which is used in the Dunham expansion of the potential (section 3.2.1.3):

$$\xi = \frac{r - r_e}{r_e},$$

ξ describes the separation of the hydrogen nuclei from equilibrium position relative to each other. The isotropic part of the polarizability is:

$$\bar{\alpha} = \bar{\alpha}_0 + \bar{\alpha}'\xi + \frac{1}{2}\bar{\alpha}''\xi^2 + ... \tag{6.9}$$

The anisotropic part, γ is:

$$\gamma = \gamma_0 + \gamma'\xi + \frac{1}{2}\gamma''\xi^2 + ..., \tag{6.10}$$

$$\bar{\alpha}_0 = \bar{\alpha}(\xi = 0), \qquad \bar{\alpha}' = \frac{\partial\bar{\alpha}}{\partial\xi}|_{\xi=0}, \text{ etc.} \tag{6.11}$$

Knippers expresses the intensity of a pure vibrational transition from the ground state to some excited state as:

$$I_{\nu\leftarrow 0} \propto F(\nu) \times \sum_{M,M'} \frac{1}{2J+1} |\langle \nu, J, M'|\alpha_{j,k}|\nu = 0, J, M\rangle|^2, \tag{6.12}$$

where the factor $(2J + 1)^{-1}$ is to account for double counting in the sum over the M quantum numbers, $F(\nu)$ is a frequency prefactor, $\alpha_{j,k}$ is the polarizability matrix element which depends on the hydrogen vibrational state and is directly proportional to the induced dipole moment as seen in Eq. 6.1. We neglect any change in the electric field from the MOF due to the change in the hydrogen vibrational state which might change the induced dipole moment. It is a secondary effect, so can be ignored. A temperature dependent factor that would describe the population of various states at equilibrium is absorbed into the proportionality of Eq. 6.12. At the temperatures of our experiment it is reasonable to assume that virtually all hydrogen molecules are in the vibrational ground state (as described in chapter 3.5). All molecules should also be in the J=0 rotational ground state. However, the limited speed of ortho to para conversion leads to a significant population of the J=1 rotationally excited state. As Knippers shows it is possible to separate Eq. 6.12 into a contribution from the isotropic, $\bar{\alpha}$, and anisotropic γ parts of the polarizability using the tensor nature of α:

$$I_{\nu\leftarrow 0} \propto F(\nu) \times \left(|\langle \nu, J|\bar{\alpha}|\nu = 0, J\rangle|^2 + \frac{7}{45} S_J |\langle \nu, J|\gamma|\nu = 0, J\rangle|^2 \right), \tag{6.13}$$

where $S_J = J(J+1)/(2J+3)(2J-1)$. Because the Q(0) is isotropic the S_J term is zero in this case and thus the anisotropic γ term does not contribute.

We now compare our results to the predictions using matrix elements calculated for molecular hydrogen. Using Eq. 6.13 and noting that for the Q(0) transition J=0 and $S_J = 0$, the expression becomes:

$$I_{\nu\leftarrow 0} \propto \nu \times |\, \langle \nu, J|\bar{\alpha}|\nu = 0, J\rangle \,|^2, \tag{6.14}$$

since $F(\nu) = \nu$ for infrared spectroscopy [60]. Many authors have calculated the necessary matrix elements for gas phase hydrogen and we summarize the results below.

TABLE 6.2: A comparison of relative intensities of the Q(0) transition in the overtone and fundamental. As described in equation 6.14 the intensity is dependent on the matrix element $\langle \nu, J|\bar{\alpha}|\nu = 0, J\rangle$. Both for H_2 in the gas phase as predicted by theory and our observed relative intensity for adsorbed H_2. Only H_2 is used since the spectra of D_2 and HD in the fundamental region do not result in clear peaks.

Reference	$\langle 20\|\bar{\alpha}\|00\rangle$	$\langle 10\|\bar{\alpha}\|00\rangle$	$I_{2\leftarrow 0}/I_{1\leftarrow 0}$
Expansion (Eq. 6.18)	N/A	N/A	1/63
Schwartz [59]	-0.0711	0.7883	1/61.46
Bishop[a] [58]	-0.0639	0.7168	1/62.92
Bishop[b] [58]	-0.0652	0.7171	1/60.48
MOF-5 experiment	N/A	N/A	1/(2.5±0.5)

a) experimental numbers

b) theoretical numbers

It is apparent that that our results differ by an order of magnitude from the ab initio calculated matrix elements. Interestingly the secondary Q(0) overtone (Fig. 5.7) is lower in intensity by a factor of 1/(125±20) which is the same order of magnitude as the theoretical predictions. To understand this amplification of the primary peaks and the consequences for the hydrogen-MOF interaction we now explore an approach that utilizes the expansion of α presented by Knippers [22]. To solve for the relative intensity we refer back to Eq. 3.28 where the vibrational wavefunctions, obtained by solving the Schrödinger equation for the anharmonic oscillator Hamiltonian, are written in terms of simple harmonic oscillator wavefunctions. Here the hydrogen is in the potential (Eq. 3.37):

$$U(\xi) = a_0(\xi^2 + a_1\xi^3 + a_2\xi^4 + ...), + U_{cd}(\xi),$$

where a_1 is significant as the coefficient for the anharmonic term of the Hamiltonian, and U_{cd} is the correction due to vibrational rotational coupling. The vibrational wavefunctions depend on B_e and ω_e which are the rotational and vibrational molecular constants. Townes summarizes the mass dependence of all molecular constants, making the point that if they are measured for one isotopologue their values for other isotopologues can

be found using these relations:

$$\omega_e \propto \frac{1}{\sqrt{\mu}} \qquad B_e \propto \frac{1}{\mu} \qquad \alpha_e \propto \frac{1}{\mu^{3/2}}, \tag{6.15}$$

where α_e is a measure of the rotational and vibrational coupling and indicates how the rotational constant changes with vibrational state. Here μ is the reduced mass, where $\mu_{D_2} = 2\mu_{H_2}$ and $\mu_{HD} = 4\mu_{H_2}/3$ as shown in Eq. 3.11 and Eq. 3.12. Our examination of intensity takes advantage of these relations.

Using these solutions Knippers derives that the intensity for the fundamental Q(0) transition:

$$I_{1\to 0} = F(\nu) \times \frac{B_e}{\omega_e}\bar{\alpha}'^2, \tag{6.16}$$

which has a $1/\sqrt{\mu}$ dependence. The intensity for the overtone vibrational transition is:

$$I_{2\to 0} = F(\nu) \times \frac{1}{2}\left(\frac{B_e}{\omega_e}\right)^2 \times \left(\bar{\alpha}'' + a_1\bar{\alpha}'\right)^2, \tag{6.17}$$

and has a $1/\mu$ dependence. The relative intensity of the overtone versus the fundamental is:

$$\frac{I_{2\to 0}}{I_{1\to 0}} = \frac{B_e}{\omega_e}\left(a_1 + \frac{\bar{\alpha}''}{\bar{\alpha}'}\right)^2, \tag{6.18}$$

which has a $1/\sqrt{\mu}$ dependence. Again the frequency prefactor for intensity is ν in infrared spectroscopy [60] and since $\nu_{ov}/\nu_{fund} \approx 2$ the factor of 1/2 in Eq. 6.18 is canceled. Bishop et. al. calculate $\alpha''/\alpha' = 0.537\pm0.0002$ [58]. To a good approximation the polarizability is the same for all hydrogen isotopologues. The only difference between the isotopologues is the neutron number in the nuclei which does not effect the charge distribution. Rychlewski [61] calculates the polarizability of H_2, HD and D_2 at multiple equilibrium separation of nuclei. From his results it is apparent that $\bar{\alpha}$ differs by less than 1% at each equilibrium separation for each isotopologue with low J quantum number as in the Q(0) and Q(1) transitions. The anharmonic constant from the potential is given as: $a_1 = -(1 + \omega_e\alpha_e/6B_e^2)$ in terms of molecular constants. By referring to Eq. 6.15 we can see that a_1 does not depend on mass and thus does not depend on isotopologue, $a_1 = -1.607$, for all isotopologues [22]. Thus the only change in $\frac{I_{2\to 0}}{I_{1\to 0}}$ with isotopologue comes from the factor $\frac{B_e}{\omega_e}$, which is 0.0138 for H_2 [58] and using the known spectroscopic constants is 0.00977 for D_2 [22]. This means that the overtone should be about 100 times less intense for D_2 and about 60 times less intense for H_2.

It is apparent from table 6.2 that our overtone Q(0) peaks are greatly amplified relative to gas phase values. This is a promising result in that these peaks which are predicted to be extremely weak are only decreased in intensity by a factor of 2.5 from the fundamental spectrum. If the intensity were a factor of 60 different then it would be prohibitively

difficult to obtain our overtone spectra. Based on equation 6.18 either the anharmonicity coefficient a_1 of the potential expansion or the ratio of the second derivative of the polarizability to the first derivative α''/α' is significantly changed from gas phase. The ratio would either need to become negative or significantly larger than a_1 = -1.607 to change the relative intensity.

6.3 Rotational Peaks

We show in this section that the S(0) and S(1) peaks in our spectra are dominated by the quadrupole induction mechanism and the effect of the polarizability mechanism can be neglected. This is a consequence of the fact that the anisotropic part of the polarizability, γ while not being negligible itself, leads to predicted peaks of negligible intensity. This can be quantitatively seen by returning to the predicted relative line intensities in Raman spectroscopy [57]:

$$S(J) \propto \frac{7}{30} |\langle \nu J|\gamma|\nu' J+2\rangle|^2 K(J+1) \tag{6.19}$$

$$Q(J) \propto (2J+1)|\langle \nu J|\bar{\alpha}|\nu' J\rangle|^2 + \frac{1}{15}|\langle \nu J|\gamma|\nu' J\rangle|^2 \frac{J(J+1)(2J+1)}{(2J+3)(2J-1)} \tag{6.20}$$

$$+\left|\langle \nu J|\gamma|\nu' J\rangle\right|^2 \left(-\frac{2J+1}{9} + \frac{4}{15}K(J)\right) \tag{6.21}$$

$$K(J) = \frac{J(J+1)}{(2J+1)} \tag{6.22}$$

Using matrix elements from [59] this predicts from the polarizability mechanism that S(0) is approximately 9 % as intense as Q(0) in the fundamental and S(1) is approximately 16 % as intense as Q(0). Our data are clearly inconsistent with these predictions since both S peaks are actually more intense than the Q(0) peak in the fundamental region 5.1. Thus we can conclude that the S peak intensities arise mainly from the Quadrupole mechanism. The strong S peaks that allow for this approximation are an unusual feature of MOF-5 and do not occur in other materials as shown in Fig. 6.2.

For the ease of calculation we now proceed as if the entire S peak intensity arises from the quadrupole induction mechanism. From this assumption we can treat the quadrupole induction mechanism similarly to how we treated the polarizability mechanism. First we examine the intensity of a transition from the ground vibrational state $\nu = 0$:

$$I_{\nu\leftarrow 0,\ J+2\leftarrow J} = |\langle 0JM|DQ_{H_2}(\theta,\phi)|\nu J'M'\rangle|^2. \tag{6.23}$$

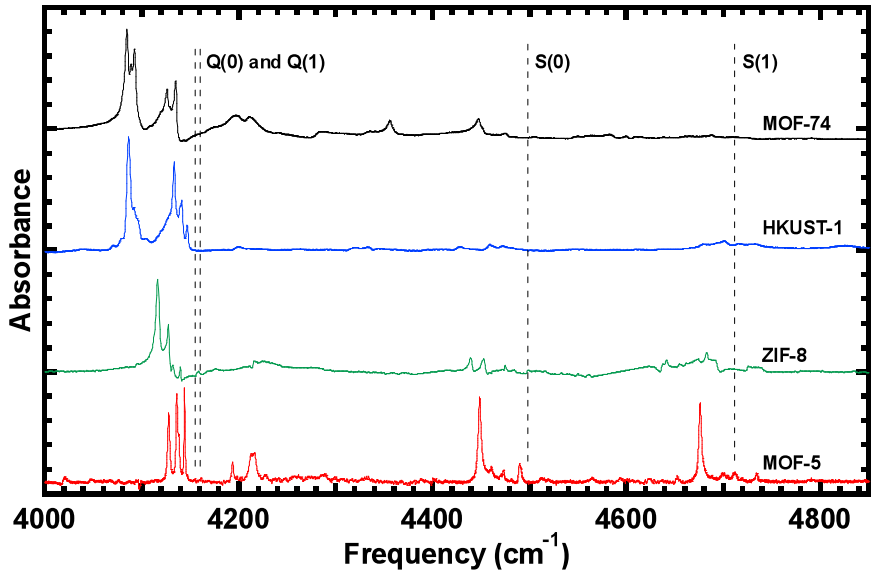

FIGURE 6.2: Typical spectra of adsorbed hydrogen, showing the fundamental region of H_2 in a range of materials, demonstrating the unusually high relative intensity of the S peaks to Q peaks in MOF-5. Spectra taken by previous students in the FitzGerald group.

If we assume that rotations and vibrations are separable we can write this as:

$$I_{\nu\leftarrow 0,\ J+2\leftarrow J} = D^2 |\langle 0|Q(\xi)|\nu\rangle|^2 \times \sum_{MM'} |\langle JM|f(\theta,\phi)|J+2M'\rangle|^2. \tag{6.24}$$

The degeneracy has been lifted since now we only sum over the M' quantum numbers that produce a distinct peak in our spectra. However since we are only interested in the ratio of like transitions in the fundamental and overtone region the M dependent term cancels out. Thus we can write it as a constant which depends on J without being concerned about its actual value:

$$I_{\nu\leftarrow 0,\ J+2\leftarrow J} = D_J^2 \ \left|\langle 0|Q(\xi)|\nu\rangle\right|^2 \tag{6.25}$$

We now write the quadrupole as an expansion in ξ:

$$Q = Q_e + Q'_e\xi + \frac{1}{2}Q''_e\xi^2. \tag{6.26}$$

Notice the similarity to the Q(0) intensity in the previous section. Since this has the same dependence on ξ and no J dependence it can be solved in the same way as in section 6.2 to arrive at a similar prediction for relative intensity for the S(J) transitions in the overtone versus fundamental:

$$\frac{I_{2\to 0}}{I_{1\to 0}} = \frac{B_e}{\omega_e}\left(a_1 + \frac{Q''_e}{Q'_e}\right)^2. \tag{6.27}$$

TABLE 6.3: A comparison of relative intensities of the S(0) and S(1) transition in the overtone and fundamental. This is both for H_2 in the gas phase as predicted by theory and our observed relative intensity for adsorbed H_2. Only H_2 is used since the spectra of D_2 and HD in the fundamental region do not result in clear peaks. Note that there is a factor of two definition difference between Poll et. al. [62] and Karl et. al. [63]. To account for this we have multiplied the results from Karl by two. Experimental numbers are obtained from fitting peaks in Fig. 6.1

Reference	$\langle 00\|Q\|12\rangle$	$\langle 00\|Q\|22\rangle$	$\langle 01\|Q\|13\rangle$	$\langle 01\|Q\|23\rangle$	$I\frac{S_2(0)}{S_1(0)}$	$I\frac{S_2(1)}{S_1(1)}$
Expansion	N/A	N/A	N/A	N/A	1/19	1/19
Karl [63]	0.1568	-0.0234	0.1442	-0.0236	1/22.5	1/18.7
Poll [62]	0.15666	-0.023285	0.14409	-0.023652	1/22.633	1/18.557
Experiment	N/A	N/A	N/A	N/A	1/(17±1)	1/(22±4)

We obtained values for Q_e'' and Q_e' by fitting the quadrupole moment as a function of internuclear separation calculated by Poll et. al. [62].

The good agreement with theory for the relativity intensities of the S peaks obtained using the IR spectrum of trapped hydrogen in MOF-5 (table 6.3) suggests that the quadrupole mechanism is not significantly changed from gas phase while the polarizability mechanism for hydrogen at the metal site is given the much larger overtones of the Q(0) peak than predicted.

6.4 Q(1) Transition

We now turn our attention to the Q(1) transition which is an effect of both the quadrupole induction mechanism and the polarizability mechanism. We note that the intensity is:

$$I_{\nu\leftarrow 0}Q(1) = \left|\langle \nu, 1, M|\mu_{sys}|0, 1, M'\rangle\right|^2, \tag{6.28}$$

since we cannot now neglect any part of the total dipole moment given in Eq. 6.4. Thus we rewrite the intensity as:

$$I_{\nu\leftarrow 0}Q(1) = \left|\langle \nu, 1, M|C\alpha_{H_2} + DQ_{H_2}(\theta,\phi)|0, 1, M'\rangle\right|^2. \tag{6.29}$$

This can now be expanded

$$\begin{aligned} I_{\nu\leftarrow 0}Q(1) = {} & C^*C\left|\langle \nu, 1, M|\alpha_{H_2}|0, 1, M'\rangle\right|^2 + D^*D\left|\langle \nu, 1, M|Q_{H_2}(\theta,\phi)|0, 1, M'\rangle\right|^2 \\ & + C^*D\,\langle \nu, 1, M|\alpha_{H_2}|0, 1, M'\rangle^*\,\langle \nu, 1, M|Q_{H_2}(\theta,\phi)|0, 1, M'\rangle \\ & + D^*C\,\langle \nu, 1, M|Q_{H_2}(\theta,\phi)|0, 1, M'\rangle^*\,\langle \nu, 1, M|\alpha_{H_2}|0, 1, M'\rangle\,. \end{aligned} \tag{6.30}$$

The first two terms can be evaluated as we did in the previous two sections. However the second two terms, the cross terms, are intractable as we do not even know their sign or whether they add or subtract to the whole intensity. It is still illustrative to explore the

TABLE 6.4: A comparison of relative intensities of the Q(1) transition in the overtone and fundamental, both for H_2 in the gas phase as predicted by theory for both mechanisms separately, and our observed relative intensity for adsorbed H_2. Again only H_2 is used since the spectra of D_2 in the fundamental region do not result in clear peaks.

Reference	$I_{2\leftarrow0}/I_{1\leftarrow0}$	Mechanism (Matrix Element)
Schwartz [59]	1/60	Polarizability
Poll [62]	1/31	Quadrupole
Karl [63]	1/30	Quadrupole
MOF-5 Q(1)	1/(14±3)	Both
MOF-5 Q(0)	1/(2.5±0.5)	Polarizability
MOF-5 S(1)	1/(22±4)	Quadrupole

predictions for the relative intensity if the Q(1) was purely as result of the polarizability mechanism or the quadrupole induction mechanism. We summarize these predictions in table 6.4. The experimental numbers do not agree with theory for either mechanism. This indicates that there is as expected a combination of both mechanisms. The Q(0) peak intensity which is purely a result of the polarizability mechanism is a factor of 1/2.5 down from the fundamental to the overtone. The rotational, S peaks, which are dominated by the quadrupole induction mechanism, are approximately a factor of 1/20 down. The Q(1) is a factor of 1/14 down which is reasonably between the two effects and is consistent with being a combination of the two mechanisms.

So to summarize we see that while it is possible that the unusual intensity of the Q(0) overtone could be an effect of the DRIFTS technique it seems unlikely since the Q(0) and Q(1) are so close in frequency - only about 15 cm^{-1} apart. If DRIFTS were responsible we would expect to see the same amplification in the Q(1), which is not observed. It is improbable that a frequency dependent effect would vary on such a short range.

One could also argue that the $Q_1(0)/Q_2(0)$ relative intensity is an effect of a suppression of the Q(0) peak in the fundamental region. However the fact that the S(1) is suppressed in the overtone relative to the Q(1), $I_{Q_1(1)}/I_{S_1(1)} = 0.77\pm0.04$ while $I_{Q_2(1)}/I_{S_2(1)} = 1.5\pm0.55$, indicates that this is not the case.

It could also be that the H_2 molecule itself is significantly perturbed, but this is inconsistent with the near-perfect agreement of the frequencies with the Buckingham predictions as described in section 5.1.

The relative intensity of the S peaks in the overtone agreeing so well with predictions (table 6.3) could be a fortuitous coincidence but it is highly suggestive that the quadrupole induction mechanism term is behaving as expected from theory for free hydrogen.

Therefore it appears that the polarizability mechanism term has had its anharmonicity greatly increased while leaving all other terms consistent with free hydrogen theory and thus not significantly perturbed. This points to an intriguing modification of the hydrogen molecule that is yet unresolved. Possible explanations could center around non-linear effects in that the hydrogen at the metal site, about 3.6 Å away from the metal [28], experiences both a very large electric field on the order of 10^{10} V/m and a large gradient in the electric field.

Chapter 7

Further Work

7.1 Translational Peaks in the Overtone

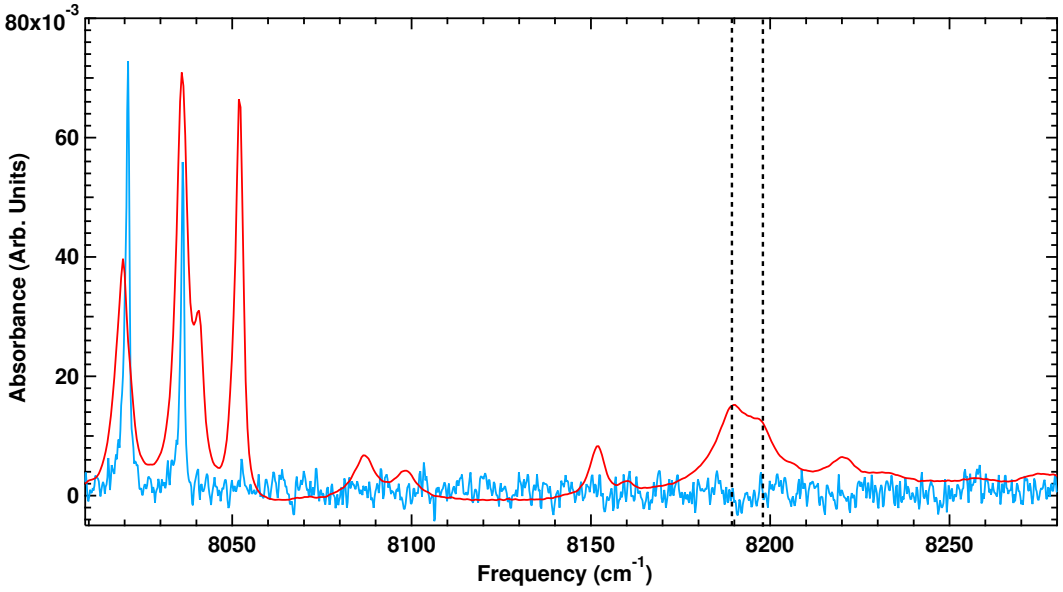

FIGURE 7.1: Spectra showing lack of translational peaks in the overtone. The primary region spectrum (red) has been scaled down by a factor of 1/10 and plotted over the overtone spectrum (blue). The translational peaks would need to be suppressed by a factor of at least 1/50 to be within the noise. This is in contrast to the Q(0) which is a factor of 1/2.5 less intense in the overtone and Q(1) which is suppressed by a factor of 1/14.

One of the remaining mysteries is why in our overtone spectrum we see no peaks due to the translational transitions (described in section 3.2.3). One possible explanation is to say that the translational sideband in the fundamental region is due mainly to the quadrupole induction mechanism. Then it might, like the S peaks, be greatly reduced in the overtone to be within the noise (Fig. 7.1).

7.2 Ortho to Para Conversion

In the future we would like to extend the work done on ortho to para conversion using the overtone as a new and powerful probe of the conversion rate. It is possible that the long time required for the pressure in these materials to come to total equilibrium due to hydrogen molecules 'hopping' from site to site could distort our ortho to para ratio. Thus we would like to perform a control experiment using HD which does not exhibit the o-p conversion. In HD the nuclei are not identical thus no molecules are trapped in the J=1 state. This is both expected theoretically and confirmed in our spectra when we see only one vibrational peak (Fig. 5.4). Therefore any change in the HD peak intensity over time at constant temperature and concentration would purely be due to the change in number of molecules occupying the primary metal site and not due to conversion.

We would also like to probe the timescale of D_2 conversion. As stated in section 3.4 at room temperature D_2 has a 1:2 ratio of more J=0 molecules than J=1. This ratio is eventually expected to come to mainly J=0 molecules but with a much slower rate than H_2 in molecular solids [41]. Since the overtone spectra D_2 is resolved and not over complicated by MOF-5 peaks it might be possible to obtain a timescale for D_2 conversion which is predicted to be about seven times slower than H_2 conversion [42]. However the rate at which the system, the MOF and the hydrogen, loses energy or relaxes from the J=1 to J=0 state could be shorter for D_2 simply because the energy being dissipated is proportional to the rotational constant which has a one over reduced mass dependence and thus is small for D_2. Thus experimentally measuring a rate of conversion would be of much experimental and theoretical interest to understanding the mechanism of o-p conversion in adsorbed hydrogen in MOF-5.

7.3 Rotational Splitting

As seen in Fig. 5.3 there appears to be some splitting of the $S_2(0)$ D_2 and HD transition. In the fundamental region it is possible that this is false and due only to MOF-5 confusion. In the clean overtone spectrum it is more intriguing. We would like to do further work, using the InGaAs detector (described in section 4.1.3) to study the HD S(0) overtone. However as there are no easily available filters to use in the region unlike the H_2 Q(0) overtone, we are working on building a broader than usual monochromator that would provide a tunable frequency window of about 100 cm^{-1} with which we could study both the HD overtone and other regions in extensive detail.

Chapter 8

Conclusion

For the first time we have measured the overtones of H_2, HD and D_2 in the material MOF-5. We found that parts of the overtone spectrum are much more intense and thus more useful than expected for understanding the behavior of trapped gases The overtone spectrum provides a new tool to study the behavior of trapped hydrogen and has allowed for the study of the H_2 isotopologue spectrum in MOF-5. The intensity of transitions dominated by the quadrupole induction mechanism agree reasonably well with theory formulated for gaseous hydrogen. The intensity of transitions dominated by the polarizability mechanism are greatly enhanced over what is expected in the overtone. This suggests some interesting modification of the hydrogen polarizability when trapped in the MOF. Now that we have demonstrated the feasibility of studying the overtone spectrum there are possibilities to apply this technique to other materials and perhaps other gases. Gases such as carbon dioxide and methane are infrared active which means that residual gas phase peaks complicate the spectrum in the fundamental region [64–66]. However, if as in H_2 the adsorbed overtone spectrum of these gases is greatly enhanced relative to gas phase the spectrum would become much clearer.

Appendix A

Appendix A

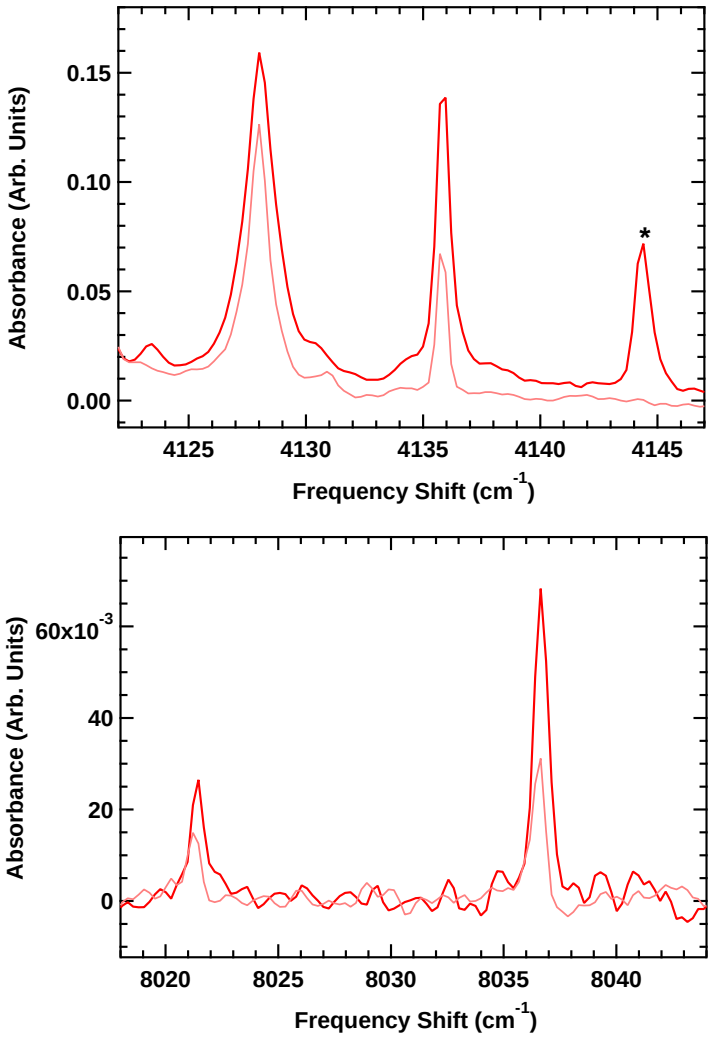

FIGURE A.1: Unscaled vibrational bands of H_2 both in fundamental region (top) and overtone region (botton). Spectra are shown at concentrations of 0.2 (light) and 0.7 (dark) hydrogens per metal. The two panels show different portions of the same spectra, the width of both regions is 25 cm^{-1}.

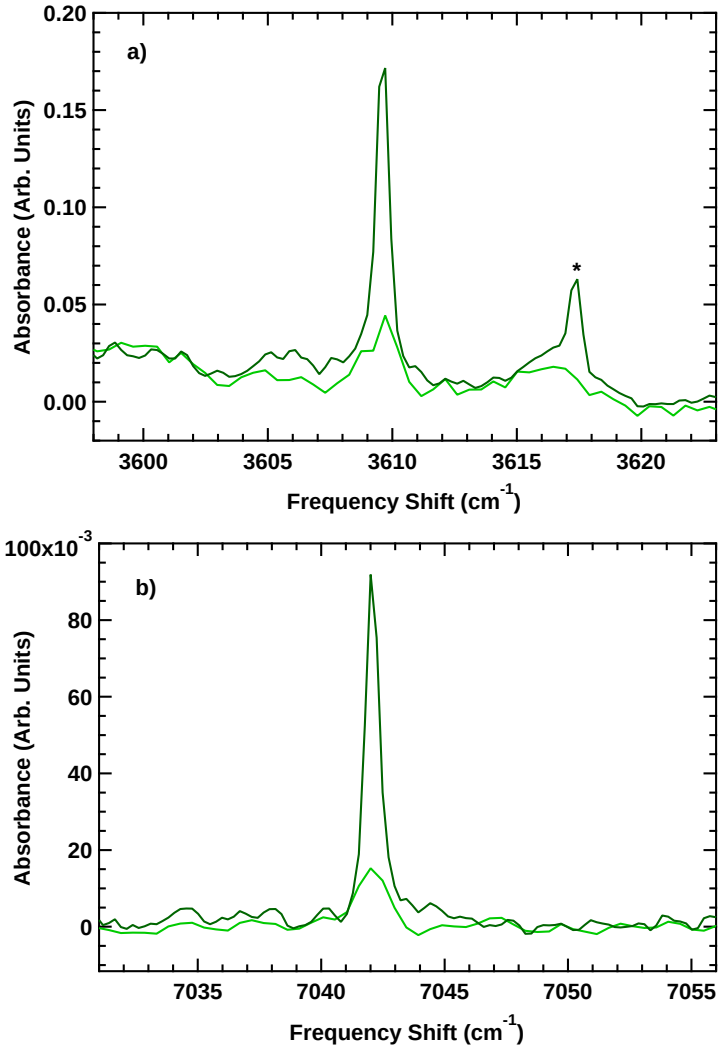

FIGURE A.2: Unscaled vibrational bands of HD both in fundamental region (top) and overtone region (botton). Spectra are shown at concentrations of 0.2 (light) and 0.7 (dark) hydrogens per metal. The two panels show different portions of the same spectra. The width of both regions is 25 cm^{-1}.

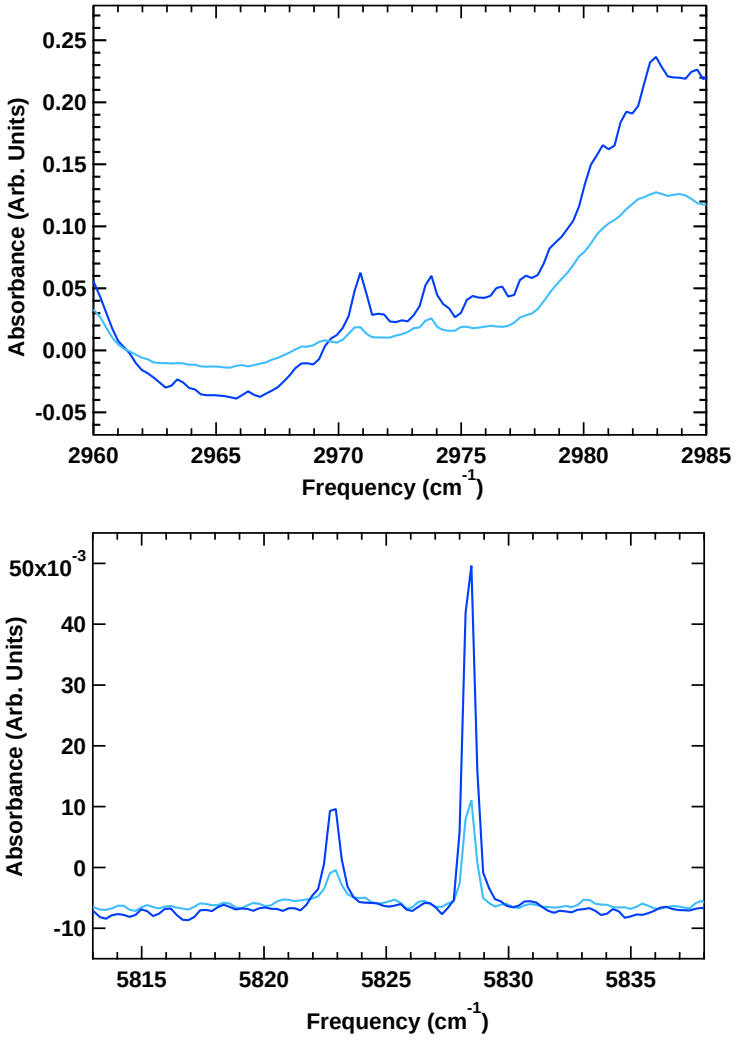

FIGURE A.3: Unscaled vibrational bands of D_2 both in fundamental region (top) and overtone region (bottom). Spectra are shown at concentrations of 0.2 (light) and 0.7 (dark) hydrogens per metal. The two panels show different portions of the same spectra with the exception of the 0.7 hydrogen/Zn concentration D_2 overtone for which a broadband filter (described in section 4.1.3) was used. The width of both regions is 25 cm^{-1}.

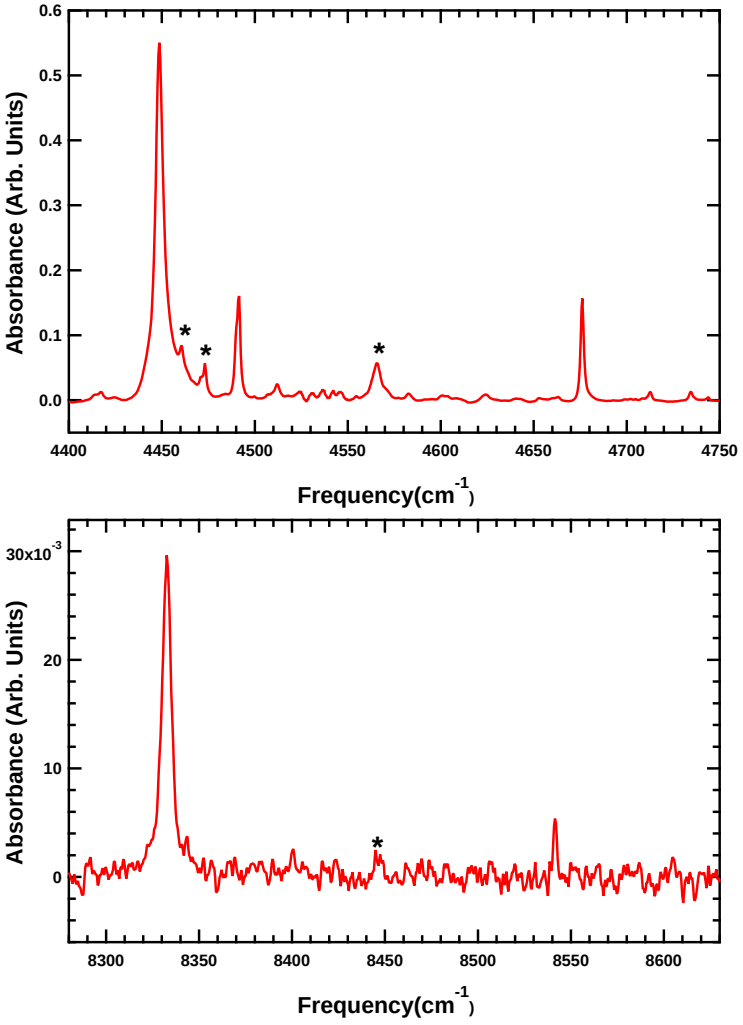

FIGURE A.4: Unscaled rovibrational bands of H_2 both in fundamental region (top) and overtone region (bottom). Spectra are at a concentrations of 0.9 hydrogens per metal. The two panels show different portions of the same spectra. The width of both regions is 350 cm^{-1}, stars indicate areas where the MOF-5 background spectrum did not correctly cancel out.

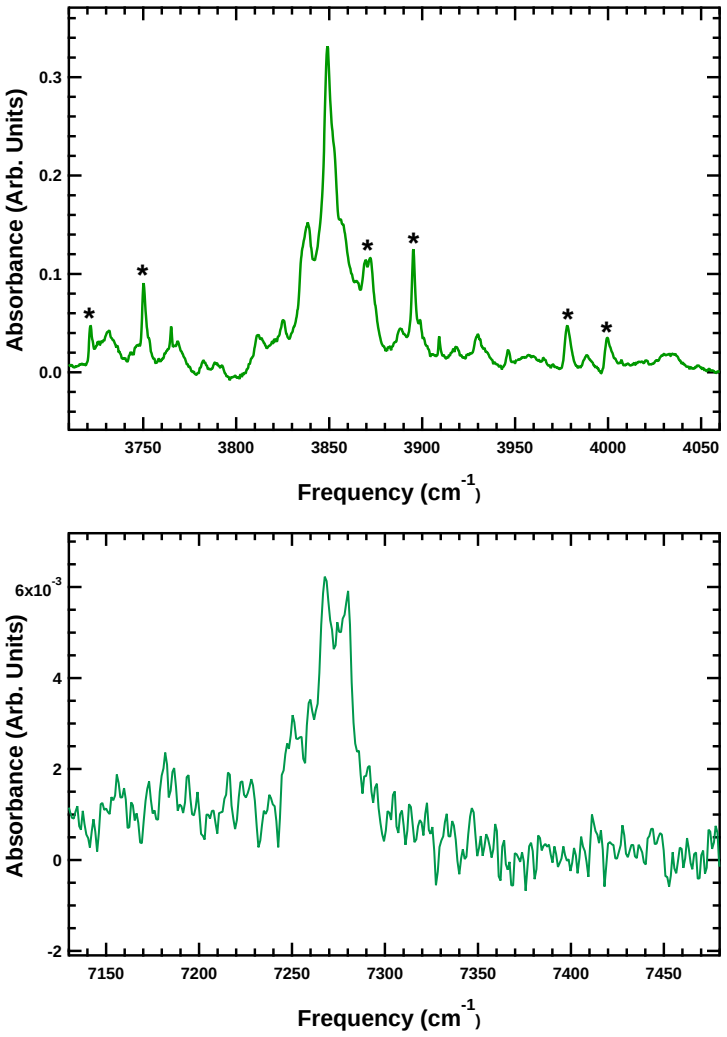

FIGURE A.5: Unscaled rovibrational bands of HD both in fundamental region (top) and overtone region (bottom). Spectra are at a concentrations of 0.7 HD/Zn in the fundamental and 0.9 HD/Zn in the overtone. The width of both regions is 350 cm^{-1}, stars indicate areas where the MOF-5 background spectrum did not correctly cancel out.

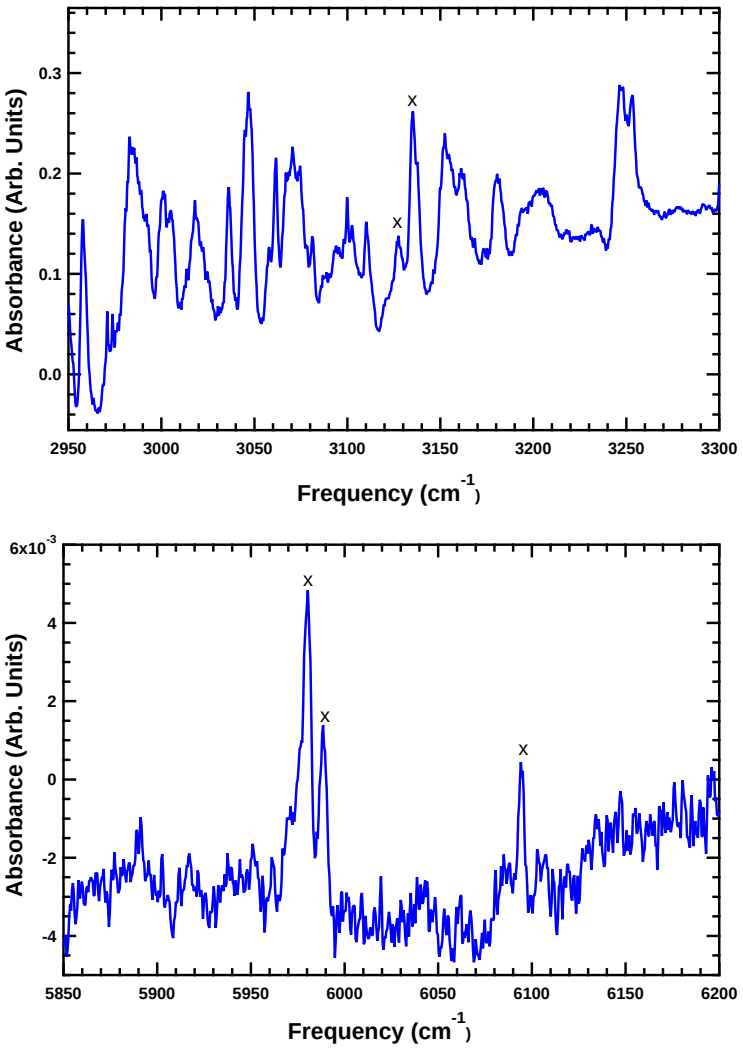

FIGURE A.6: Unscaled rovibrational bands of D_2 both in fundamental region (top) and overtone region (bottom). Spectra are at a concentrations of 0.7 D_2/Zn. The width of both regions is 350 cm^{-1}, x indicates adsorbed D_2 peaks in order to distinguish them from the MOF-5 spectra not canceling out.

Bibliography

[1] C. J. Pierce. Quantum sieving of h_2 and d_2 in fe-mof-74, 2012. URL http://new.oberlin.edu/departments/physics/documents/projects/honors/PierceThesis2012.pdf.

[2] S. A. FitzGerald, C. J. Pierce, J. L. C. Rowsell, E. D. Bloch, and J. A. Mason. Highly selective quantum sieving of d2 from h2 by a metal-organic framework as determined by gas manometry and infrared spectroscopy. *J. Am. Chem. Soc.*, 135 (25):94589464.

[3] H. Oh, I. Savchenko, A. Mavrandonakis, T. Heine, and M.. Hirscher. Highly effective hydrogen isotope separation in nanoporous metal-organic frameworks with open metal sites: Direct measurement and theoretical analysis. *ACS Nano*, 8(1):761–770, 2014.

[4] *Understanding and Responding to Climate Change*, 2008. United States National Academy of Sciences.

[5] K. L. Lim, H. Kazemian, Z. Yaakob, and W. R. W. Daud. Solid-state materials and methods for hydrogen storage: A critical review. *Chem. Eng. Technol*, 33(2): 213–226, 2010.

[6] March 2014. URL http://webbook.nist.gov/cgi/fluid.cgi?Action=Load&ID=C1333740&Type=SatT&Digits=5&PLow=.5&PHigh=1.5&PInc=.1&RefState=DEF&TUnit=K&PUnit=atm&DUnit=kg/m3&HUnit=kJ/mol&WUnit=m/s&VisUnit=uPa*s&STUnit=N/m#Liquid.

[7] U. S. Department of Energy. Targets for onboard hydrogen storage systems for light-duty vehicles us department of energy office of energy efficiency and renewable energy and the freedomcar and fuel partnership. 2009.

[8] A. Goncharov, A. Guglya, and E. Melnikova. On the feasibility of developing hydrogen storages capable of adsorption hydrogen both in its molecular and atomic states. *International Journal of Hydrogen Energy*, 37:18061–18073, 2012.

[9] M. Felderhoff, C. Weidenthaler, R. von Helmolt, and U. Eberle. Hydrogen storage: the remaining scientific and technological challenges. *Phys. Chem. Chem. Phys.*, 9 (2643-2653), 2007.

[10] M. P. Suh, H. J. Park, T. K. Prasad, and D. Lim. Hydrogen storage in metal-organic frameworks. *Chem. Rev.*, 112(782-835), 2012.

[11] S. Li and Q. Xu. Metal-organic frameworks as platforms for clean energy. *Energy Environ. Sci.*, 6:1656–1683, 2013.

[12] L. J. Murray, M. Dinca, and J. R. Long. Hydrogen storage in metal-organic frameworks. *Chem. Soc. Rev*, 38:1294–1314, 2009.

[13] T. Duren, Y. Bae, and R. Q. Snurr. Using molecular simulation to characterise metal-organic frameworks for adsorption application. *Chem. Soc. Rev.*, 38:1237–1247, 2008.

[14] L Kong, Y. J. Chabal, and D. C. Langreth. First-principles approach to rotational-vibrational frequencies and infrared intensity for h_2 adsorbed in nanoporous materials. *Physical Review B*, 83:121402, 2011.

[15] S. A. FitzGerald, K. Allen, P. Landerman, J. Hopkins, J. Matters, R. Myers, and J. L. C. Rowsell. Quantum dynamics of adsorbed h_2 in the microporous framework mof-5 analyzed using diffuse reflectance infrared spectroscopy. *Physical Review B*, 77(22):9, 2008.

[16] C. O. Aren, S. Chavan, C. P. Cabello, E. Garrone, and G. T. Palomino. Thermodynamics of hydrogen adsorption on metal-organic frameworks. *ChemPhysChem*, 11:3237?3242, 2010.

[17] S. Bordiga, L. Regli, F. Bonino, E. Groppo, C. Lamberti, B. Xiao, P. S. Wheatley, R. E. Morris, and A. Zecchina. Adsorption properties of hkust-1 toward hydrogen and other small molecules monitored by ir. *Physical Chemistry Chemical Physics*, 9(21):2676–2685, 2007.

[18] S. Bordiga, J. G. Vitillo, G. Ricchiardi, L. Regli, D. Cocina, A. Zecchina, B. Arstad, M. Bjorgen, J. Hafizovic, and K. P. Lillerud. Interaction of hydrogen with mof-5. *Journal of Physical Chemistry B*, 109(39):18237–18242, 2005.

[19] L. Z. Kong, V. R. Cooper, N. Nijem, K. H. Li, J. Li, Y. J. Chabal, and D. C. Langreth. Theoretical and experimental analysis of h2 binding in a prototypical metal-organic framework material. *Physical Review B*, 79(8):081407–081411, 2009.

[20] N. Nijem, L. Z. Kong, Y. G. Zhao, H. H. Wu, J. Li, D. C. Langreth, and Y. J. Chabal. Spectroscopic evidence for the influence of the benzene sites on tightly bound h-2 in metal-organic frameworks with unsaturated metal centers: Mof-74-cobalt. *Journal of the American Chemical Society*, 133(13):4782–4784, 2011.

[21] D. P. Shelton. Raman overtone intensities measured for h_2. *J. Chem. Phys.*, 93(3): 1491–1495, August 1990.

[22] W. Knippers, K. Vanhelvoort, and S. Stolte. Vibrational overtones of the homonuclear diatomics (n_2, o_2, d_2) observed by the spontaneous raman effect. *Chemical Physics Letters*, 121(4-5):279–286, 1985.

[23] S. L. Bragg, J. W. Brault, and W. H. Smith. Line positions and strengths in the h_2 quadrupole spectrum. *The Astrophysical Journal*, 263:999–1004, December 1982.

[24] H. Bose, H. Forester, and W. Frede. Induced overtones of homonuclear diatomics in zeolitic materials. *Chem. Phys. Lett.*, 138(5):401–404, 1987.

[25] K. Beck, H. Pfeifer, and B. Staudte. Diffuse reflectance fourier-transform infrared studies of hydrogen adsorbed on sodium zeolites. *J. Chem. Soc. Faraday Trans.*, 89 (21):3995–3998, 1993.

[26] V. B. Kazansky, V. Yu. Borovkov, and H. G. Karge. Diffuse reflectance ir study of molecular hydrogen and deuterium adsorbed at 77 k on naa zeolite part 2. overtone, combination and vibrational-rotational modes and thermodesorption from naa zeolite. *INTERNATIONAL JOURNAL OF RESEARCH IN PHYSICAL CHEMISTRY AND CHEMICAL PHYSICS*, 211:1–12, 1999.

[27] Elinor C. Spencer, Judith A. K. Howard, Garry J. McIntyre, Jesse L. C. Rowsell, and Omar M. Yaghi. Determination of the hydrogen absorption sites in zn4o(1,4-benzenedicarboxylate) by single crystal neutron diffraction. *Chem Communications*, pages 278–280, December 2006.

[28] T. Yildirim and M. R. Hartman. Direct observation of hydrogen adsorption sites and nanocage formation direct observation of hydrogen adsorption sites and nanocage formation in metal-organic frameworks. *Physical Review Letters*, 95:215504–1–4, November 2005.

[29] Jesse L. C. Rowsell, Elinor C. Spencer, Juergen Eckert, Judith A. K. Howard, and Omar M. Yaghi. Gas adsorption sites in a large-pore metal-organic framework. *Science*, 309(5739):1350–1354, August 2005.

[30] A. G. Wong-Foy, A. J. Matzger, and O. M. Yaghi. Exceptional h_2 saturation uptake in microporous metal-organic frameworks. *Journal of American Chemical Society*, 128:3494–3495, 2006.

[31] H. Li, M. Eddaoudi, M. O'Keeffe, and O. M. Yaghi. Design and synthesis of an exceptionally stable and highly porous metal-organic framework. *Nature*, 402, 1999.

[32] Jesse. B. Hopkins. Infrared spectroscopy of h_2 trapped in metal organic frameworks, 2009. URL http://new.oberlin.edu/departments/physics/documents/projects/honors/Thesis_finalHopkins.pdf.

[33] J. L. C. Rowsell, J Eckert, and O. M. Yaghi. Characterization of h_2 binding sites in prototypical metal-organic frameworks by inelastic neutron scattering. *Journal of American Chemical Society*, 127:14904–14910, 2005.

[34] G. Herzberg. *Molecular Spectra and Molecular Structure*, volume I - Spectra of Diatomic Moecules. Prentice-Hall Inc, 1945.

[35] David J. Griffiths. *Introduction to Quantum Mechanics*. Pearson Prentice Hall, 2nd edition, 2005.

[36] H. Hamaguchi, A. D. Buckingham, and W. J. Jones. Determination of derivatives of the polarizability anisotropy in diatomic-molecules .2. the hydrogen and nitrogen molecules. *Molecular Physics*, 43(6):1311–1319, 1981.

[37] B. P. Stoicheff. High resolution raman spectroscopy of gasses, ix. spectra of h_2, hd and d_2. *Canadian Journal of Physics*, 35:730–741, January 1957.

[38] A. L. Schawlow C. H. Townes. *Microwave Spectroscopy*. Dover Publication Inc, 1975.

[39] C. N Banwell and E. M. McCash. *Fundamentals of Molecular Spectroscopy*. McGraw-Hill Book Company, 1994.

[40] E. U. Condon. Production of infrared spectra with electric fields. *Physical Review*, 41:759–762, 1932.

[41] I. F. Silvera. The solid molecular hydrogens in the condensed phase: Fundamentals and static properties. *Rev. Mod. Phys.*, 52(2):393–452, April 1980.

[42] K. Fukutani and T Sugimoto. Physisorption and ortho-para conversion of molecular hydrogen on solid surfaces. *Progress in Surface Science*, 88:279–348, 2013.

[43] Christie Simmons. The quantum dynamics of h_2 in a c60 lattice, 2005. URL http://new.oberlin.edu/arts-and-sciences/departments/physics/documents/projects/honors/Simmons_honors.pdf.

[44] Peter R. Griffiths and A. de Haseth. *Fourier Transform Infrared Spectroscopy*. John Wiley and Sons, 1986.

[45] S. A. FitzGerald, H. O. H. Churchill, P. M. Korngut, C. B. Simmons, and Y. E. Strangas. Cryogenic apparatus for diffuse reflection infrared spectroscopy with high-pressure capabilities. *Review of Scientific Instruments*, 77(9):4, 2006.

[46] H. Hamaguchi, I. Suzuki, and A. D. Buckingham. Determination of derivatives of the polarizability anisotropy in diatomic-molecules .1. theoretical considerations on vibration-rotation raman intensities. *Molecular Physics*, 43(4):963–973, 1981.

[47] S. Kassi and A. Campargue. Electric quadrupole and dipole transitions of the first overtone band of hd by crds between 1.45 and 1.33 μm. *Journal of Molecular Spectroscopy*, pages 36–42, March 2011.

[48] S. Kassi, A. Campargue, K. Pachucki, and J. Komasa. The absorption spectrum of d_2: Ultrasensitive cavity ring down spectroscopy of the (2-0) band near 1.7 μm and accurate ab initio line list up to 24 000 cm^{-1}. *J. Chem. Phys.*, 136, May 2012.

[49] A. D. Buckingham. Solvent effects in vibrational spectroscopy. *The Faraday Society and Contributors*, pages 753–760, January 1960.

[50] S. A. FitzGerald, B. Burkholder, M. Friedman, J. B. Hopkins, C. J. Pierce, J. M. Schloss, B. Thompson, and J. L. C Rowsell. Metal-specific interactions of h_2 adsorbed within isostructural metal-organic frameworks. *J. Am. Chem. Soc.*, 133: 20310–20318, 2011.

[51] S. A. FitzGerald, J. Hopkins, B. Brukholder, and M. Friedman. Quantum dynamics of adsorbed normal- and para-h_2, hd, and d_2 in the microporous framework mof-74 analyzed using infrared spectroscopy. *Phys. Rev. B*, 81:104305, 2010.

[52] G. Buntkowsky, B. Walaszek, A. Adamczyk, Y. Xu, H. Limbach, and B. Chaudret. Mechanism of nuclear spin initiated para-h_2 to ortho-h_2 conversion. *Phys. Chem. Chem. Phys.*, 8(16):1929–1935, 2006.

[53] Brian S. Burkholder. Catalysis of conversion between the spin isomers of h_2 by mof-74, 2009. URL http://new.oberlin.edu/departments/physics/documents/projects/honors/Thesis_Burkholder.pdf.

[54] E. Ilisca. Hydrogen conversion on non-magnetic insulating surfaces. *European Physics Letters*, 104:18001, 2013.

[55] R. M. Herman and J. C. Lewis. Theory of the fundamental vibration-rotation-translation spectrum of h-2 in a c-60 lattice. *Phys. Rev. B.*, 73(15), April 2006.

[56] K. E. Kerr, T. Momose, D. P. Weliky, C. M. Gabrys, and T. Oka. Condon modulation spectroscopy of solid hydrogen and measurement of the temperature-dependence of the q1(0) transition. *Phys. Rev. Lett.*, 72(25):3957–3960, June 1994.

[57] T. C. James and W. Klemperer. Line intensities in the raman effect of diatomic molecules. *Journal of Chemical Physics*, 31(1):130–134, 1959.

[58] D.M. Bishop and J. Pipin. Calculated raman overtone intensities for h_2 and d_2. *J. Chem. Phys.*, 94(9):6073–6080, May 1991.

[59] C. Schwartz and R. J. Le Roy. Nonadiabatic eigenvalues and adiabatic matrix elements for all isotopes of diatomic hydrogen. *J. Molec. Spec.*, 121:420–439, 1987.

[60] E. B. Wilson, J. C. Decius, and P. C. Cross. *Molecular Vibrations the Theory of Infrared and Raman Vibrational Spectra*. Dover Publications, 1955.

[61] J. Rychlewski. An accurate calculation of the polarizability of the hydrogen molecule an dits dependence on rotation, vibration and isotopic substitution. *Molecular Physics*, 41(4):833–842, 1980.

[62] J. D. Poll and L. Wolniewicz. The quadrupole moment of the h_2 molecule. *J. Chem. Phys*, 68(7):3053–3058, April 1978.

[63] G. Karl and J. D. Poll. On the quadrupole moment of the hydrogen molecule. *J. Chem. Phys*, 46(8):2944–2950, 1967.

[64] N. Nijem, P. Canepa, U. Kaipa, K. Tan, K. Roodenko, S. Tekarli, J. Halbert, I. W. H. Oswald, R. K. arvapally, C. Yang, T. Thronhauser, M. A. Omary, and Y. J. Chabal. Water cluster confinement and methane adsorption in the hydrophobic cavities of a fluorinated metal-organic framework. *J. Am. Chem. Soc.*, 135(34): 12615–12626, August 2013.

[65] N. Nijem, P. Canepa, L. Z. Kong, Wu. H. H., J. Li, T. Thronhauser, and Y. J. Chabal. Spectroscopic characterization of van der waals interactions in a metal organic framework with unsaturated metal centers: Mof-74-mg. *J. Phys. Condens. Matter.*, 24(42), October 2012.

[66] Y. Zhao, H. Wu, T. J. Emge, Q. Gong, N. Nijem, Y. J. Chabal, L. Kong, D. C. Langreth, H. Liu, H. Zeng, and J.] Li. Enhancing gas adsorption and separation capacity through ligand functionalization of microporous metal-organic framework structures. *Chem. Eur. J.*, 17(18):5101–5109, April 2011.